Early prediction of preeclampsia in pregnancy with circulating cell-free RNA

Mira N. Moufarrej[1], Sevahn K. Vorperian[2], Ronald J. Wong[3], Ana A. Campos[3], Cecele C. Quaintance[3], Rene V. Sit[4], Michelle Tan[4], Angela M. Detweiler[4], Honey Mekonen[4], Norma F. Neff[4], Maurice L. Druzin[5], Virginia D. Winn[5], Gary M. Shaw[3], David K. Stevenson[3], Stephen R. Quake[1,4,6,*]

[1] Department of Bioengineering, Stanford University, Stanford, CA USA 94305
[2] Department of Chemical Engineering, Stanford University, Stanford, CA USA 94305
[3] Department of Pediatrics, Stanford University School of Medicine, Stanford, CA USA 94305
[4] Chan Zuckerberg Biohub, Stanford, CA USA 94305
[5] Department of Obstetrics and Gynecology, Stanford University School of Medicine, Stanford, CA USA 94305
[6] Department of Applied Physics, Stanford University, Stanford, CA USA 94305

[*] Corresponding author: steve@quake-lab.org

Abstract

Liquid biopsies that measure circulating cell-free RNA (cfRNA) offer an unprecedented opportunity to noninvasively study the development of pregnancy-related complications and to bridge gaps in clinical care. Here, we used 404 blood samples from 199 pregnant mothers to identify and validate cfRNA transcriptomic changes that are associated with preeclampsia (PE), a multi-organ syndrome which is the second largest cause of maternal death globally. We find that changes in cfRNA gene expression between normotensive (NT) and preeclamptic mothers are striking and stable early in gestation, well before the onset of symptoms. These changes are enriched for genes specific to neuromuscular, endothelial, and immune cell types and tissues that reflect important aspects of PE physiology and suggest new hypotheses for disease progression. This enabled identification and independent validation of a panel of 18 genes whose measurement between 5–16 weeks of gestation can form the basis of a liquid biopsy test that would identify mothers at risk of PE well before the clinical symptoms manifest themselves. Finally, we demonstrate that cfRNA changes reflect the multifactorial nature of PE and provide a means to non-invasively monitor maternal organ health. Tests based on these observations could help predict and manage who is at risk for PE, an important and until now unachieved objective for obstetric care.

Introduction

Advances in obstetrics and neonatology have significantly mitigated many of the adverse pregnancy outcomes related to preterm birth (PTB) and preeclampsia (PE) [1,2]. Nonetheless, the standards of care implemented today focus on how to treat a mother and child once a complication has been diagnosed, proving both insufficient and costly [3–6]: PE and related hypertensive disorders cause 14% of maternal deaths each year globally, second only to hemorrhage [7], and cost nearly $2B in care in the first year following delivery [5]. Worse, 3 out of 5 maternal deaths in the US are preventable and often associated with a missed or delayed complication diagnosis [8]. Such outcomes highlight the need for novel tools that would aid in identifying which mothers are at risk for hypertensive diseases, such as PE, before clinical presentation. Indeed, early prediction, which

has not been achieved to date, may enable prevention or reduction of a pregnant mother's risk of developing PE [9,10] if coupled with appropriate treatment.

PE is a leading pregnancy-related complication that globally affects 4–5% of pregnancies [11–13] and is associated with a significant increase in adverse maternal and perinatal outcomes [14–18]. Long-term, PE presents an increased maternal risk for cardiovascular [19,20] and kidney [21,22] diseases. Formally defined as new-onset hypertension with proteinuria or other organ damage (e.g., liver, brain) occurring after 20 weeks of gestation [23], PE can clinically manifest anytime thereafter, including into the post-partum period [24]. Detection and diagnosis have proven challenging both because early signs such as headaches and nausea can be easily confused with generalized pregnancy discomfort and because PE shares many signs and symptoms with other common complications like gestational thrombocytopenia and chronic hypertension.

To date, no recommended test exists that can predict the future onset of PE early in pregnancy [9]. Investigational approaches that measure biochemical signals including the measurement of two angiogenic factors (soluble fms-like tyrosine kinase-1 (sFlt1), placental growth factor (PlGF)) in the second and third trimesters [25,26] have at best only moderate positive predictive values (8–33%) [27]. A clinical test could guide the prophylactic use of low-dose aspirin, which has been shown to safely reduce the risk of PE if initially administered before 16 weeks of gestation [10,28,29]. Liquid biopsies that measure plasma cell-free RNA (cfRNA) suggest a means to bridge this gap in clinical care; however, until recently, such work often failed to progress beyond initial discovery [30]. Recent efforts have instead either focused on confirmation of PE at clinical diagnosis [31,32] or on limited individuals earlier in pregnancy with encouraging but unvalidated results [33]. Consequently, the prediction of PE early in gestation, before symptoms present, when such a test would be most useful to guide the prophylactic use of potential therapeutics remains a key objective to improve obstetric care [9].

Clinical care may also be improved by a better understanding of PE's pathogenesis. PE is which is specific to humans [34] and a few non-human primates [35], and consequently, elucidating its pathogenesis has proved challenging. Broadly, it is accepted that PE occurs in two stages – abnormal placentation early in pregnancy followed by systemic endothelial dysfunction [15,34,36]. Because PE can clinically present any time after 20 weeks of gestation and with a diversity of symptoms, significant effort has been made to subclassify the disease based upon the timing of onset as a proxy for pathology [37,38]; however, debate over the significance of such subtyping is ongoing [34,36,39,40]. Separate efforts have focused on subtyping PE molecularly using placental gene expression and histology [41,42]. Since cfRNA is derived from many tissues in the body [43,44], noninvasive liquid biopsies present a potential means to indirectly observe pathogenesis in real time and to identify physiological changes associated with PE for proposed subtypes both prior to and at diagnosis.

Here, we report that cfRNA transcriptomic changes can distinguish between normotensive (NT) and PE pregnancies throughout the course of pregnancy, irrespective of PE subtype. Interestingly, the majority of these cfRNA changes are most striking early in pregnancy – well before the onset of symptomns - suggesting that the identified cfRNA signal may correlate with PE pathogenesis, which is thought to also occur at this time. Indeed, gene ontology (GO) and tissue and cell type of origin analyses identified pathways, tissues, and cell types that both reflect known PE physiology

and suggest new means to stratify the disease. These observations enabled us to identify and independently validate a panel of 18 genes that when measured between 5–16 weeks of gestation form a predictive signature of which mothers are at risk for developing PE. Finally, we demonstrate that cfRNA signals reflect the multifactorial nature of PE and provide a means to noninvasively monitor maternal organ health. Taken together, these results show that cfRNA measurements can form the basis for clinically relevant tests that would predict PE months before presentation, manage who is at risk for specific organ damage, and help characterize the pathogenesis of PE in real time.

Results

Clinical study design

To identify changes associated with PE well before traditional diagnosis, we designed a prospective study and recruited pregnant mothers at their first clinical visit to Stanford's Lucile Packard Children's Hospital, between 5–12 weeks of gestation, of which 131 were included in this study (94 NT, 37 with PE). For each participant, we analyzed cfRNA for samples collected before or at 12 weeks, between 13-20 weeks, and at or after 23 weeks of gestation, and post-partum (0–4 weeks after delivery). We then split this larger group into Discovery (n = 88, [60 NT, 28 with PE]) and Validation 1 (n = 43, [34 NT, 9 with PE]) cohorts. We also obtained samples from an independent cohort collected at several separate institutions (Validation 2), which consisted of 89 samples collected prior to 16 weeks of gestation from 87 mothers (61 NT, 26 with PE) (Fig 1A).

For all cohorts, we included individuals of diverse racial and ethnic backgrounds in approximately matched proportions across NT and PE groups (Table S1). We recorded maternal pre-pregnancy and pregnancy characteristics, and defined a pregnancy as NT if it was both uncomplicated and went to full-term (≥ 37 weeks) or as PE with or without severe features based on current guidelines (see Methods). For mothers who developed PE, all antenatal blood samples were collected prior to diagnosis.

Our final analysis included a subset of those samples which passed pre-defined quality metrics (Supp. note 1, Methods, Fig S1). After confirming sample quality, 404 samples from 199 mothers (142 NT, 57 with PE) were included in the final analysis (Table S2). Specifically, 209, 106, and 89 samples from 73, 39, and 87 participants (49, 32, 61 NT; 24, 7, 26 with PE) were included in Discovery, Validation 1, and Validation 2, respectively (RNAseq).

Across gestational timepoints in all cohorts, we found no significant difference in sampling time between PE and NT groups ($p \geq 0.26$, 0.11, 0.46). Known risk factors for PE, such as pre-pregnancy maternal body mass index (BMI), maternal age, and gravidity followed expected trends. BMI specifically was significantly different between PE and NT groups in Discovery cohort alone ($p = 0.02$, 0.45, NA) while maternal age and gravidity were not ($p \geq 0.29$, 0.16, 0.2) (Fig 1B, Table S1). History of PTB and mode of delivery were significantly different between NT and PE groups only for Validation 2. Other demographic factors like race, ethnicity, and nulliparity differed across cohorts but not between case groups within each cohort (adjusted $p \leq 0.05$, chi-squared test for categorical or ANOVA for continuous variables with Bonferroni correction, Table S1).

137 In mothers who later developed PE, we observed no significant difference (p = 0.14, 1.0, 0.4) in
138 gestational age at onset between those who did not experience severe symptoms (n = 11, 4, 3*) as
139 compared with those with did experience severe (n = 13, 3, 13*) symptoms (Fig 1C). Furthermore,
140 21 mothers who developed PE also delivered preterm (n = 9, 1, 11) as compared with no mothers
141 in the NT group as reflected by significantly different gestational ages at delivery ($p = 10^{-7}$, 0.04,
142 10^{-9}, one-sided test) (Fig 1D) and lower fetal weight at delivery (Table S1), which was consistent
143 with epidemiological evidence that PE increases the risk of spontaneous or indicated preterm
144 delivery [5,27] (values reported as Discovery, Validation 1, Validation 2, Mann-Whitney rank test
145 unless otherwise specified, * denotes data were incomplete for specified cohort).
146
147 *Identification of cfRNA changes across gestation in mothers who developed PE*
148
149 There were 544 differentially expressed genes (DEGs) that differed across gestation and post-
150 partum between mothers who later developed PE with or without severe features as compared with
151 NT mothers who did not experience complications (adjusted $p \leq 0.05$, see Methods and
152 Supplementary Note 2). Most DEGs (498) were annotated as protein-coding, and a small fraction
153 (43, 8%) were other types including 11 mitochondrial t-RNAs, 6 long non-coding RNAs, 8
154 pseudogenes, and 1 small nucleolar RNA (snoRNA).
155
156 To further understand when these changes occur during gestation, we estimated the log fold-
157 change (logFC) for each gene by each gestational time point as well as post-partum. We observed
158 that these gene changes occurred most strikingly before 20 weeks of gestation as indicated by a
159 clear bimodal distribution with two peaks centered around logFC of +0.8 and -0.6 (Fig 2A). We
160 also found that gene changes were also most stable before 20 weeks of gestation where over 50%
161 of genes had a coefficient of variation (CV) < 1 as compared to 31% at or after 23 weeks of
162 gestation and 36% at post-partum (Fig S2A).
163
164 We then asked whether a subset of gene changes approximately proportional in number to total
165 sample number (n = 49, 49, 57, 46 for each time point) was sufficient to segregate PE (n = 13, 16,
166 20, 17) and NT (n = 36, 33, 37, 29) samples across gestation. We found that 24-32 genes were
167 sufficient to separated PE and NT samples across gestation and at post-partum with good
168 specificity (86% [75–93%], 79% [66–88%], 97% [90–100%], and 90% [78–96%]) and sensitivity
169 (85% [64–95%], 88% [69–96%], 65% [47–80%], and 71% [51–86%]) (Fig 2B, S2B, All values
170 reported for ≤12 weeks, 13-20 weeks, ≥23 weeks of gestation and post-partum, [90% CI]) (See
171 also Fig S3, File S1).
172
173 Nearly all 544 DEG changes showed excellent agreement in both Validation cohorts as compared
174 to Discovery across gestation but not post-partum. Specifically, more than 82% and 92% of genes
175 across gestation had the same logFC sign with a spearman correlation of at least 0.67 and 0.71 for
176 Validation 1 and 2 respectively ($p<10^{-15}$) as compared with 60% and 0.35 post-partum (Fig 2C,
177 S2C). Finally, we asked whether symptom severity (without or with severe features) correlated
178 with logFC magnitude for these 544 DEGs common to both PE subtypes. We found that on
179 average, symptom severity did not influence logFC magnitude as reflected by a slope of nearly 1
180 across gestation and post-partum (Fig S2E).
181
182 *cfRNA changes reflect disease pathophysiology in mothers who developed PE*

The 544 identified DEGs could be well categorized into two longitudinal trends (Fig 2D, S4A,C). Resembling a valley or V-shape, the first trend (Group 1) described the longitudinal behavior of 216 genes (40%), for which measured levels were reduced in PE samples (-1.3x to -1.5x) across gestation with a minimum between 13–20 weeks. Peaking in early gestation before 20 weeks (1.75x), the second trend (Group 2) described the behavior of 328 genes (60%) that had significantly elevated levels in PE samples before 20 weeks and to a lesser extent after 23 weeks of gestation (1.3x). For Group 1 but not 2, gene changes were far less evident post-partum and trended toward no difference between PE and NT, which may reflect a placental contribution to DEG levels.

Approximately 13% of DEGs were tissue or cell-type specific (Fig 2E). Genes that were decreased in PE across gestation (Group 1) were broadly enriched for the immune system, whereas, those genes increased in PE across gestation (Group 2) were enriched for nervous, muscular, endothelial, and immune contributions as reflected by cell-type (adjusted $p \leq 0.05$, hypergeometric test) and pathway enrichment (adjusted $p \leq 0.05$, hypergeometric test) (Fig S2E, Table S3). Consistent with current understanding of the pathogenesis of PE, we identified a strong endothelial-linked signal underscored by contributions from capillary aerocytes ($p = 0.03$), an endothelial cell-type specific to the lungs [45], platelets ($p = 10^{-33}$), and several platelet related pathways like platelet degranulation and platelet activation, signaling, and aggregation ($p \leq 10^{-8}$) among others.

Surprisingly, we also found significant, elevated nervous and muscular contributions for PE as emphasized by contributions from excitatory neurons ($p = 0.02$), oligodendrocytes ($p = 0.005$), and smooth muscle ($p = 0.0003$) and terms like muscle contraction and dilated cardiomyopathy ($p \leq 0.02$). The immune system also contributes to both elevated (e.g., mesenchymal stem cells, total PBMCs) and decreased (granulocytes, T-cells) changes across gestation. Genes in both groups were enriched for signaling pathways (i.e., secretion by cell, integrin-mediated signaling pathway, regulation of I-kappaB kinase, NF-kappaB signaling). Group 2 was also enriched for cellular compartments such as the cell periphery, cell junctions, and extracellular space, consistent with reports that PE may be associated with signaling from the fetoplacental complex [46]. Finally, DEGs were broached enriched for genes previously implicated in PE [47] (30 gene overlap, $p = 0.006$, hypergeometric test) (Table S3).

A machine-learning classifier predicts risk of PE on or before 16 weeks of gestation

Since gene changes associated with PE pathogenesis across gestation are readily detected irrespective of symptom severity, we sought to build a classifier that could identify mothers at risk of PE at or before 16 weeks of gestation (Supplementary Note 2, Fig S2E). We trained a logistic regression model on the Discovery cohort (n = 61 NT, 24 PE samples). After training, the final model performed well with a near perfect AUROC (0.99 [0.99–0.99]), good specificity (85% [77–91%]), and perfect sensitivity (100% [92-100%]) (Fig 3A, Table 1). We then tested this model on Validation 1 (n = 35 NT, 8 PE) and two other independent cohorts, which were collected at separate institutions: Validation 2 (n = 61 NT, 28 PE samples) and Del Vecchio and colleagues [33] cohort (n = 8 NT, 5 with PE, 7 with gestational diabetes, 2 with chronic hypertension). Across these cohorts, the final model once again performed well with consistent AUROC (0.71 [0.70-0.71], 0.72 [0.71–0.72], 0.74 [0.73–0.74]), sensitivity (75% [46–92%], 56% [42-72%], 60% [26–87%]) and

229 specificity (56% [43–70%], 69% [59-78%], 100% [89–100%]) (All reported as Validation 1,
230 Validation 2, Del Vecchio) (Fig 3A, Table 1).
231
232 Next, we inspected erroneously classified samples from the Validation 2 and Del Vecchio cohorts.
233 For false negatives in Validation 2 and Del Vecchio, we find a shift to later gestational ages at
234 collection (13.5 ± 2, 12.5 ± 2 weeks) as compared to PE samples that were correctly classified (12
235 ± 2, 12 ± 0 weeks; mean ± SD for Validation 2, Del Vecchio) (Fig S5A). This suggests that in
236 practice, there may an optimal collection window to reduce false negatives. Indeed, if we only
237 consider samples before 14 weeks of gestation, we observe a 9% and 15% increase in sensitivity
238 with corresponding AUROC values of 0.73 and 0.90 for Validation 2 and Del Vecchio
239 respectively. There were no false positives in the Del Vecchio cohort, suggesting that the model
240 can distinguish between PE and other risks like chronic hypertension or gestational diabetes. The
241 model also proved well-calibrated estimating a slightly elevated probability of PE for gestational
242 diabetes (0.15 ± 0.08) and chronic hypertension (0.18 ± 0.13) – known PE risk factors [48–54] – as
243 compared to the estimate for NT samples (0.09 ± 0.08) (mean ± SD, Fig S5B). These elevated
244 probabilities for other risk factors impacted the test's AUROC (0.74 [0.73-0.74] as compared to
245 0.8 [0.79-0.8] for only PE vs NT samples, Table 1) (all reported as value, [90% CI]).
246
247 Finally, we inspected the 18 genes (Fig 3B, Table S4) used by the model to yield probability
248 estimates. Eight genes were annotated in the Human Protein Atlas (HPA)[55] as enhanced or
249 enriched in the placenta (FAM46A, MYLIP), neuromuscular (CAMK2G, NDUFV3, PI4KA,
250 PRTFDC1) and immune systems (RNF149, TRIM21). Univariate analysis further confirmed that
251 9 of the gene trends (i.e., decreased or increased gene levels in PE) observed in the Discovery
252 dataset are upheld in Validation 2 (adjusted $p \leq 0.05$, one-sided Mann-Whitney rank test) (Fig 3B).
253 We also found that the majority of models trained using a subset of the 18 initial genes can predict
254 future PE onset with varying performance. Notably, performance improved across all metrics
255 (sensitivity, specificity, and AUROC) as we increased the number of genes included for model
256 training (Table S5, Fig S5C).
257
258 *The multifactorial nature of PE and maternal organ health is reflected in cfRNA*
259 We next wondered whether cfRNA measurement reflects the multifactorial nature of PE. We
260 identified 503 DEGs (adjusted $p \leq 0.05$) that differed across gestation between mothers who later
261 developed PE with as compared to without severe symptoms. Since there were no significant
262 differences in symptom severity as related to timing of PE onset (Fig 1C), we believe that our
263 observations contrasting PE with and without severe symptoms are not obscured by differences in
264 PE-onset type. As before, most DEGs (484) were annotated as protein-coding, and a small fraction
265 (18, 4%) were other types including 12 pseudogenes and 4 long non-coding RNAs.
266
267 We observed that DEGs could be well categorized into 4 longitudinal trends (Fig 4A, S4B,D).
268 Two groups (Group 1, 3) described the temporal behavior of 217 genes (44%), for which measured
269 levels were either consistently increased (Group 1) or reduced (Group 3) in PE with as compared
270 to without severe symptoms (±1.8x) across gestation and trended towards no change post-partum.
271 In contrast, Groups 2 and 4 (286 genes, 56%) changed signs in mid-gestation beginning as slightly
272 elevated (Group 2, 1.2x) or decreased (Group 4, -1.2x) in severe PE and then moving to decreased
273 (Group 2, -1.4x) or unchanged (Group 4, 1x) at ≥23 weeks of gestation.

Analysis of the enriched cell types and tissues of origin for each of these groups revealed that elevated gene differences in severe PE were driven by contributions from endothelial cells and the adaptive immune system (bone marrow). In contrast, genes that changed signs over gestation were enriched for innate immune cell types (e.g., granulocytes and neutrophils for Group 2, thymus for Group 4) (Table S6). Quantifying total cfRNA signal confirmed an increased bone marrow signal for only severe PE across gestation and a decreased granulocyte signal for only PE without severe features at ≤12 weeks of gestation (Fig 4B). Gene ontology analysis further revealed pathways specific to genes that were only decreased for severe PE in early gestation (Group 4) like axon guidance, nervous development, and metabolism of RNA (adjusted $p < 0.05$).

We next investigated whether it might be possible to monitor organ health noninvasively focusing on eight organ systems (Fig 4B) relevant to PE presentation with consequences such as proteinuria, impaired liver function, renal insufficiency, and epilepsy. We found striking shifts in total contributions for all systems. We observed an increased astrocyte signal before 20 weeks of gestation and decreased oligodendrocytes and excitatory neurons at ≥23 weeks of gestation for all PE relative to NT (Fig 4B, 1st row). Although placental contributions increased over pregnancy with a peak in late gestation as expected, placental tissue and syncytiotrophoblast contributions were reduced for PE pregnancies before 20 weeks of gestation. Finally, we observed a decreased signal in hepatocyte, kidney, endothelial cell, and smooth muscle signatures across gestation and increased platelet signal before 12 weeks of gestation for PE. These tissue and cell type specific changes are both consistent with common PE pathogenesis and the specific, prominent diagnoses in our cohort (e.g., thrombocytopenia, proteinuria, impaired liver function, renal insufficiency).

Discussion

Noninvasive measurements of the cf-transcriptome present an opportunity to study human development and disease from any organ at a molecular scale. Here, we showed that circulating cfRNA measurements taken during pregnancy can clearly distinguish between PE and NT pregnancies. We found that the most striking differences occur early on and broadly showed no reproducible difference at post-partum, consistent with known PE etiology, namely that the placenta drives the disease process [34,36]. We next validated these changes using two separate cohorts (Validation 1 and 2) and explored their physiological relevance.

Our findings provide molecular evidence supporting generally accepted physiological understanding of PE pathogenesis: early abnormal placentation and systemic endothelial dysfunction [34]. Early in gestation, we observe a reduced placental signal for PE regardless of onset type or symptom severity. Concurrently, platelets and endothelial cells drive cfRNA changes in all PE as compared to NT and between PE with or without severe symptoms especially before 20 weeks of gestation. Increases in cell-type specific cfRNA may occur through signaling and secretion by cells, as underscored by functional enrichment analysis. The innate and adaptive immune system also heavily contribute to cfRNA changes in PE with clear, marked shifts related to bone marrow, T-cells, B-cells, granulocytes, and neutrophils, consistent with previous studies on the maternal-placental interface and PE [34,56–58] .

PE is a broad and complex syndrome. Because the complication can present clinically across more than 20 weeks with a diversity of symptoms, significant effort has been made to subclassify the disease based on timing of onset. Used as a proxy for hypothesized pathogenesis, the timing of PE

320 onset subdivides the disease into 'placental' early-onset PE (occurring before 34 weeks of
321 gestation) and 'maternal' late-onset PE (occurring on or after 34 weeks) [34,37,59]. However, early-
322 and late-onset PE may represent a spectrum of disease severity that corresponds with timing of
323 onset and may lead to additional pregnancy complications, such as intrauterine growth restriction
324 (IUGR) [34,36,38,39]. Indeed, some evidence such as transcriptional profiling of whole blood drawn at
325 diagnosis suggests a common gene signature for both subtypes [40]. Our findings further corroborate
326 a common signature across onset types and suggest that PE may be better stratified based on
327 symptom severity.
328
329 Indeed, PE may be best subtyped molecularly. Given the diversity of clinical presentations, we
330 propose a novel, noninvasive means of monitoring a mother's risk of specific organ damage,
331 common in PE. The cfRNA changes we characterized here reflect dysfunction in at least five organ
332 systems (brain, liver, kidney, muscle, bone marrow), and can in some cases further distinguish
333 between PE with or without severe symptoms. As a molecular lens into maternal health, liquid
334 biopsies present an opportunity as both a research and clinical tool to learn about the pathogenesis
335 of a human disease in humans and as a predictor of maternal health. Here, we have shown proof
336 of principle that cfRNA measurements can form the basis for a robust liquid biopsy test, which
337 predicts PE very early in gestation and if validated in controlled clinical studies, could help
338 discover and manage those at risk for PE. Such a test could serve as a complement to recent efforts
339 based on clinical and laboratory data[60], and even be coupled with tests taken later during gestation.
340 We further demonstrated that cfRNA measurements reflect who is at risk for specific organ
341 damage. Together, these results form the basis for a series of clinical tests that can be used to help
342 characterize and stratify the pathogenesis of PE in real time, to date unrealized key objectives for
343 obstetric care.
344

Acknowledgements. We thank N. Aghaeepour and I. Maric from Stanford University for helpful discussion and data analysis suggestions, the many researchers and clinicians affiliated with the March of Dimes Prematurity Research Center at Stanford University for insightful feedback after oral presentations, and the participants in this study for their invaluable contribution.

Funding. This work was supported by the Chan Zuckerberg Biohub and the March of Dimes Foundation. M.N.M. is supported by the Stanford Bio-X Bowes Fellowship. S.K.V. is supported by a NSF Graduate Research Fellowship (Grant # DGE 1656518), the Benchmark Stanford Graduate Fellowship, and the Stanford ChEM-H Chemistry Biology Interface (CBI) training program. V.D.W. is supported by the H&H Evergreen Fund.

Author contributions. M.N.M., G.M.S., D.K.S., and S.R.Q. conceptualized and designed this study. M.L.D., V.D.W., G.M.S., and D.K.S. designed the cohort study at Lucile Packard Children's Hospital. R.J.W., A.A.C., and C.C.Q. collected and processed whole blood samples and corresponding sample and participant metadata. GAPPS oversaw, collected, and processed whole blood samples and corresponding sample and participant metadata at GAPPS. M.N.M. developed experimental protocols for cfRNA extraction and data generation and processed all samples from cfRNA extraction up to and including RT-qPCR and library generation for RNA sequencing. R.V.S., M.T., A.D., H.M., and N.F.N. developed and executed experimental protocols for RNA sequencing and computational protocols for raw sequencing data transfer. S.K.V. developed computational methods to define genes as cell-type and tissue specific in the context of the whole body. M.N.M and S.K.V. designed the analyses to characterize tissue and cell type contributions. M.N.M. conceptualized and developed computational analyses, analyzed the data, and wrote the initial manuscript draft in collaboration with S.R.Q.. All authors contributed to the writing and editing the manuscript.

Competing interests. The authors declare the following competing interests: M.N.M., S.K.V., G.M.S., D.K.S., and S.R.Q. are inventors on a patent application submitted by the Chan Zuckerberg Biohub and Stanford University that covers noninvasive early prediction of preeclampsia and monitoring maternal organ health over pregnancy. S.R.Q. is a founder, consultant, and shareholder of Mirvie. M.N.M. is also a shareholder of Mirvie.

Materials & methods

Clinical study design

Discovery and Validation 1 were collected as part of a longitudinal, prospective study. We enrolled pregnant mothers (aged 18 years or older) receiving routine antenatal care on or prior to 12 weeks of gestation at Lucile Packard Children's Hospital at Stanford University, following study review and approval by the Institutional Review Board (IRB) at Stanford University (#21956). All signed informed consent prior to enrollment. Whole blood samples for plasma isolation were then collected at three distinct timepoints during their pregnancy course and once (or twice for 2 individuals) post-partum.

Validation 2 was collected as part of the Global Alliance to Prevent Preterm and Stillbirth (GAPPS) at several, independent sites. Samples were processed and sequenced at Stanford under the same IRB as above (#21956). All signed informed consent prior to enrollment. Whole blood

samples for plasma isolation were collected at a single time point (or 2 timepoints in the case of 2 individuals with PE) prior to or at 16 weeks of gestation.

For all three cohorts, we ensured that all included individuals did not have chronic hypertension or gestational diabetes. Mothers were defined as having PE based upon current American College of Obstetrics and Gynecology (ACOG) guidelines (see below). Mothers were defined as controls if they had uncomplicated term pregnancies and either normal spontaneous vaginal or caesarean deliveries. For mothers who developed PE, all antenatal samples included in this study were collected prior to clinical diagnosis.

We tested for within cohort (NT vs PE) and across cohort differences in demographic variables using a chi-squared test and ANOVA for categorical and continuous variables respectively. We then applied Bonferroni correction and reported any differences as significant if adjusted $p \leq 0.05$.

Definition of PE

PE was defined per the ACOG guidelines [27] based on two diagnostic criteria: 1) new-onset hypertension developing on or after 20 weeks of gestation and 2) new-onset proteinuria or in its absence, thrombocytopenia, impaired liver function, renal insufficiency, pulmonary edema, or cerebral or visual disturbances.

New-onset hypertension was defined when the systolic and/or diastolic blood were at least 140 or 90 mmHg, respectively, on at least 2 separate occasions between 4 hours and 1 week apart. Proteinuria was defined when either 300 mg protein was present within a 24-hour urine collection or an individual urine sample contained a protein/creatinine ratio of 0.3 mg/dL, or if these were not available, a random urine specimen had more than 1 mg protein as measured by dipstick. Thrombocytopenia, impaired liver function, and renal insufficiency were defined as a platelet count of < 100,000/μL, liver transaminases ≥ 2x of normal, and serum creatinine > 1.1 mg/dL, respectively.

Symptoms were defined as severe per the ACOG guidelines. Specifically, PE is defined as severe if any of the following symptoms were present and diagnosed as described above: new-onset hypertension with systolic and/or diastolic blood pressure of at least 160 or 110 mmHg respectively, thrombocytopenia, impaired liver function, renal insufficiency, pulmonary edema, new-onset headache unresponsive to medication and unaccounted for otherwise, or visual disturbances.

Finally, a pregnant mother was considered to have early-onset PE if onset occurred before 34 weeks of gestation and late onset thereafter.

Sample preparation

Plasma processing

At Lucile Packard Children's Hospital, blood samples were collected in either EDTA-coated (Cat No 368661, Becton-Dickinson) or Streck cfRNA BCT (Cat No 218976, Streck) tubes at ≤12, 13–20, and ≥23 weeks of gestation, and post-partum for each participant. Within 30 minutes, tubes were then centrifuged at 1600g for 30 minutes at room temperature. Plasma was transferred to 2-mL microfuge tubes and centrifuged at 13000g for another 10 minutes in a microfuge. One

437 milliliter aliquots were then transferred to 2-mL Sarstedt screw cap microtubes (Cat No 50809242,
438 Fisher Scientific) and stored at -80˚C until analysis.
439
440 At GAPPS, blood samples were collected in EDTA-coated tubes at ≤16 weeks of gestation from
441 a network of collection sites including Yakima Valley Memorial Hospital, Swedish Medical
442 Center, and the University of Washington Medical Center. Per Standard Operating Procedure
443 (SOP), tubes were then centrifuged within 2 hours of collection at 2500RPM for 10 minutes at
444 room temperature in a swinging bucket rotor. Plasma was transferred to 2-mL cryovials in at most
445 1 mL aliquots and stored at -80˚C until analysis. Sample volume was also recorded.
446
447 ***cfRNA isolation***
448 In 96-sample batches, cfRNA from 1-mL plasma samples was extracted in a semi-automated
449 fashion using the Opentrons 1.0 system and Norgen Plasma/Serum Circulating and Exosomal
450 RNA Purification 96-Well Kit (Slurry Format) (Cat No 29500, Norgen). Samples were
451 subsequently treated with Baseline-ZERO DNAse (Cat No DB0715K, Lucigen) for 20 minutes at
452 37˚C. DNAse-treated cfRNA was then cleaned and concentrated into 12 µL using Zymo RNA
453 Clean and Concentrator-96 kits (Cat No R1080).
454
455 Following cfRNA extraction from plasma samples, isolated RNA concentrations were estimated
456 for a randomly selected 11 samples per batch using Bioanalyzer RNA 6000 Pico Kit (Cat No 5067-
457 1513, Agilent) per manufacturer instructions.
458
459 ***Sequencing library preparation***
460 cfRNA sequencing libraries were prepared with SMARTer Stranded Total RNAseq Kit v2 - Pico
461 Input Mammalian Components (Cat No 634419, Takara) from 4 µL of eluted cfRNA according to
462 the manufacturer's instructions. Samples were barcoded using SMARTer RNA Unique Dual Index
463 Kit – 96U Set A (Cat No 634452, Takara), and then pooled in an equimolar fashion and sequenced
464 on Illumina's NovaSeq platform (2x75 bp) to a mean depth of 54, 33, and 38 million reads per
465 sample for Discovery, Validation 1, and Validation 2 cohorts, respectively. Some samples (12, 61,
466 0 for Discovery, Validation 1, and Validation 2 cohorts) were not sequenced due to failed library
467 preparation.
468
469 **Sequencing data analysis**
470 ***Bioinformatic processing***
471 For each sample, raw sequencing reads were trimmed using Trimmomatic (v 0.36) and then
472 mapped to the human reference genome (hg38) with STAR (v 2.7.3a). Duplicate reads were then
473 removed by GATK's (v 4.1.1) MarkDuplicates tool. Finally, mapped reads were sorted and
474 quantified using htseq-count (v 0.11.1) generating a counts table (genes x samples). Read statistics
475 were estimated using FastQC (v 0.11.8).
476
477 Across samples, the bioinformatic pipeline was managed using Snakemake (v 5.8.1). Read and
478 tool performance statistics were aggregated across samples and steps using MultiQC (v 1.7).
479 Following sample quality and gene filtering, all gene counts were adjusted to $\log_2$-transformed
480 counts per million reads (CPM) with trimmed mean of M values (TMM) normalization [61].
481
482 ***Sample quality filtering***

483 For every sequenced sample, we estimated three quality parameters as previously described [62,63].
484 To estimate RNA degradation in each sample, we first counted the number of reads per exon and
485 then annotated each exon with its corresponding gene ID and exon number using htseq-count.
486 Using these annotations, we measured the frequency of genes for which all reads mapped
487 exclusively to the 3' most exon as compared to the total number of genes detected. RNA
488 degradation for a given sample can then be approximated as the fraction of genes where all reads
489 mapped to the 3' most exon. To estimate the number of reads that mapped to genes, we summed
490 counts for all genes per sample using the counts table generated from bioinformatic processing
491 above. To estimate DNA contamination, we quantified the ratio of reads that mapped to intronic
492 as compared to exonic regions of the genome.
493
494 After measuring these three metrics across nearly 700 samples, we empirically estimated RNA
495 degradation and DNA contamination's 95th percentile bound. We considered any given sample an
496 outlier, low quality sample if its value for at least one of these metrics was greater than or equal to
497 the 95th percentile bound or if no reads were assigned to genes.
498
499 Once values for each metric were estimated across the entire dataset, we visualized: (1) whether
500 low-quality samples clustered separately using hierarchical clustering (average linkage, Euclidean
501 distance metric) and (2) whether sample quality drove variance in gene measurements using
502 principal component analysis (PCA). These analyses were performed in Python (v 3.6) using
503 Scikit-learn for PCA (v 0.23.2), Scipy for hierarchical clustering (v 1.5.1), and nheatmap for
504 heatmap and clustering visualization (v 0.1.4).
505
506 ***Gene filtering***
507 We performed filtering to identify well-detected genes across the entire cohort. Specifically, we
508 used a basic cutoff that required a given gene be detected at a level of at least 0.5 CPM in at least
509 75% of discovery samples after removing outlier samples. Following this step, we retain 7,160
510 genes for DE analysis.
511
512 ***Differential expression analysis***
513 Differential expression analysis was performed in R using Limma (v 3.38.3). To identify gene
514 changes associated with PE across gestation and post-partum, we used a mixed-effects model. We
515 performed DE using two design matrices: (1) Examine the interaction between time to PE onset
516 or delivery for NT and PE symptoms (i.e., PE with or without severe symptoms) and (2) Examine
517 the interaction between time to PE onset or delivery for NT and PE broadly. In both design
518 matrices, we included time to PE onset or delivery for NT (continuous variable), whether a sample
519 was collected post-partum (binary variable), the interaction between time and PE symptoms for
520 (1) or PE for (2), the interaction between whether a sample is post-partum and PE symptoms for
521 (1) and PE for (2), and 7-8 confounding factors.
522
523 In (1), we defined PE symptoms categorially using 3 levels - NT, PE without severe symptoms,
524 PE with severe symptoms). In (2), we defined whether a sample was PE using a binary, indicator
525 variable (0 = NT, 1 = PE). The 7-8 confounding variables included were maternal race (categorial
526 variable), maternal ethnicity (binary variable), fetal sex (binary variable), maternal pre-pregnancy
527 BMI group (categorical variable), maternal age (continuous variable, only included in design 1),
528 and sequencing batch (categorical variable). We defined time to PE onset or delivery as the

529 difference between gestational age at onset or delivery and gestational age at sample collection.
530 We defined BMI group as follows: Obese (BMI ≥ 30), Overweight (25 ≤ BMI < 30), Healthy (18.5
531 ≤ BMI < 25), Underweight (BMI < 18.5). We chose to model time to PE onset or delivery as a
532 continuous variable, specifically a natural cubic spline with 4 degrees of freedom to account for
533 the range across which samples were collected (1–3 months per collection period). We also
534 blocked for participant identity (categorical variable), modeling it as a random effect to account
535 for auto-correlation between samples from the same person.
536
537 Per the Limma-Voom guide, to account for sample auto-correlation over time, we ran the function
538 voomWithQualityWeights twice. We first ran it without any blocking on participant identity, and
539 used this base estimation to approximate sample auto-correlation based on participant identity
540 using the function duplicateCorrelation. After estimating correlation, voomWithQualityWeights
541 was run again, this time blocking for participant identity and including the estimated auto-
542 correlation level. A linear model was then fit for each gene using lmFit and differential expression
543 statistics were approximated using Empirical Bayes (eBayes) methods. For comparing PE with vs
544 without severe symptoms, we contrasted the relevant coefficients (makeContrasts) and then
545 applied Empirical Bayes as opposed to directly after lmFit.
546
547 DEGs were then identified using the relevant design matrix coefficients and the function, topTable,
548 with Benjamini-Hochberg multiple hypothesis correction at a significance level of 0.05. For design
549 1, we identified DEGs related to 3 comparisons: PE without severe symptoms vs NT (1759 DEGs),
550 severe PE vs NT (1198 DEGs), and PE with vs without severe symptoms (503 DEGs). We find
551 544 genes in common for PE without and with severe symptoms vs NT. These 544 DEGs were
552 explored in Figure 2 and the related main text. For design 2, we identified DEGs related to PE vs
553 NT alone (330 DEGs), which we used as the initial gene set for building a logistic regression model
554 (see Supplementary Note 2). Finally, we removed the effect of sequencing batch alone on
555 estimated logCPM values with TMM normalization for the Discovery cohort using the limma-
556 voom function, removeBatchEffect.
557
558 ***log(Fold change) and CV estimation***
559 We define $\log_2$-transformed fold-change (logFC) as the difference between the median gene level
560 (logCPM, see Bioinformatic processing section above) between PE and NT samples for a given
561 sample collection period (i.e., ≤12, 13–20, and ≥23 weeks of gestation, or post-partum). In the case
562 where a given person had multiple samples included into a specific collection period, we only used
563 the values associated with the first collected sample to avoid artificially reducing within-group (PE
564 or NT) variance due to auto-correlation among samples from the same person.
565
566 We then quantified the relative dispersion around the estimated logFC for each gene using an
567 approximation for CV. Specifically, we consider CV to be the ratio between an error bound, ∂, and
568 the estimated logFC. We defined the error bound, ∂, as the one-sided error bound associated with
569 the lower (or upper in the case of negative logFC values) 95% CI as estimated by bootstrapping.
570 This definition of ∂ as a one-sided bound that approaches 0 (equivalent to no FC) allowed us to
571 explore how confident we could be in an estimated logFC. For instance, a CV = 1 would indicate
572 that at the boundary of proposed values, the logFC for a given gene becomes effectively 0.
573 Similarly, a CV > 1 would indicate even less confidence in a proposed average logFC and indicate

574 that at the boundary, the estimated logFC changes signs (i.e., a negative logFC becomes a positive
575 one or vice versa).
576
577 ***Hierarchical clustering analysis***
578 For each sample collection period, hierarchical clustering was performed using differentially
579 expressed genes with an |logFC| ≥ 1 and CV < 0.5 or 0.4 in the case of the 13–20 weeks of gestation
580 time point so that the number of genes used did not exceed the number of samples. For each gene
581 that passed these thresholds, we calculated a z-score across all samples (at most 1 per subject, the
582 earliest collected sample in a given group) in each sample collection period using the function
583 StandardScaler in Scikit-learn (v 0.23.2), Average linkage hierarchical clustering with a Euclidean
584 distance metric was then performed for both rows (gene z-scores) and columns (samples in same
585 collection group) for a given matrix in Python using Scipy (v 1.5.1). Clustering and corresponding
586 heatmaps were visualized using nheatmap (v 0.1.4).
587
588 ***Longitudinal dynamics analysis***
589 To group gene changes by longitudinal behavior, we performed k-means clustering on a matrix
590 where each row was a differentially expressed gene and each column was the estimated logFC for
591 a given sample collection period (N genes x 4 timepoints). We measured the sum of squared
592 distances for every 'k' between 1 and 16 (4^2) where 16 represents the maximum possible k (4
593 timepoints with 2 possibilities each, logFC > 0 or logFC < 0). We then identified the optimal k
594 clusters by using the well-established elbow method to identify the smallest 'k' that best explained
595 the data, visually described as the elbow (or knee) of a convex plot like that for the sum of squared
596 distances vs k (Fig S4A,C). To do so, we either visually inspected and identified the elbow (Fig
597 2D) or used the function KneeLocator as implemented in the package Kneed (v 0.7.0) (Fig 4A).
598 We used visual inspection for Fig 2D as we observed that given two k-values (e.g., k = 2,3) with
599 similar sum of squared distances, KneeLocator would choose the larger value whereas we
600 preferred a simpler model. Having identified the optimal number of clusters, 'k', we labeled every
601 differentially expressed gene with its assigned cluster and visualized average behavior (median)
602 and the 95% CI (bootstrapped using 1000 iterations) per cluster using Seaborn line plot (v 0.10.0).
603
604 To confirm that the identified patterns were not spurious (i.e., an artifact of the k-means clustering
605 algorithm), we permuted the data columns (logFC per timepoint) for each gene thereby scrambling
606 any time-related structure while preserving its overall distribution. We then visualized the result
607 using Seaborn line plot as described above. Following permutation, we observed no longitudinal
608 patterns, which were instead replaced by nearly flat, uninformative trends (Fig S4B,D).
609
610 ***Correlation analysis***
611 To verify DEGs identified in the Discovery cohort, we compared logFCs for the Discovery as
612 compared to both Validation 1 and Validation 2 cohorts. We calculated the percentage of genes
613 for which the logFC had the same sign across cohorts (i.e., both positive or both negative) and the
614 spearman correlation using the function scipy.stats.spearmanr. We did not calculate logFCs for
615 DEGs at ≤12 weeks of gestation in Validation 1 because of small sample numbers (3 PE samples
616 prior to 12 weeks).
617
618 We also sought to compare whether symptom severity (without or with severe) correlated with
619 logFC magnitude for 544 DEGs identified as common to all PE in design 1. To do so, we

620 calculated the slope of a best-fit line where x and y were defined as logFCs for PE without (x) and
621 with (y) severe features vs NT. We would expect a slope > 1 and < 1 if logFC magnitudes for PE
622 with as compared to without severe symptoms were larger or smaller on average respectively.
623 Similarly, a slope = 1 would reflect that symptom severity did not correlate with logFC magnitude
624 for the 544 DEGs tested.
625
626 Finally, to confirm that the identified correlations were significant, we permuted the data columns
627 (logFC per cohort) for each gene thereby scrambling any structure while preserving its overall
628 distribution. We then calculated the same statistics. Following permutation, we observe about 50-
629 55% logFC agreement, as expected at random, a spearman correlation of 0, and slope of 0.
630
631 ***Defining cell-type and tissue-specific gene profiles***
632 Cell-type and tissue specific gene profiles were all identified as previously described [44]. We also
633 briefly summarize this method below.
634
635 On the tissue level, for genes and tissues (and some blood and immune cell types) measured in the
636 Human Protein Atlas (HPA, v19)[55], we calculated a Gini index per gene as a measure of tissue
637 specificity. As a measure of inequality, Gini index values closer to 1 represent genes that are tissue
638 specific. We defined a given gene Y as specific to tissue X if Gini(Y) ≥ 0.6 and max expression
639 for Y is in tissue X. Although the aforementioned method identifies fairly tissue specific genes, it
640 is possible to have a gene Y where Gini(Y) ≥ 0.6 and the gene is expressed in more than 1 tissue
641 (e.g., enrichment in placenta and muscle). To this end, when tracking cell-type and tissue
642 trajectories over gestation (e.g., Fig 4B), where the specificity of a given gene profile is especially
643 important, we imposed a further constraint to ensure that any gene signal only reflects the named
644 tissue (e.g., any gene named placenta specific is specific to the placenta alone). Specifically, we
645 required that genes be annotated by HPA as 'Tissue enriched' or 'Tissue enhanced' and term this
646 reference, HPA strict.
647
648 On the cell-type level, we augmented Tabula Sapiens v1.0 (TSP) with cell types from missing
649 (e.g., placenta, brain), incompletely described tissues (e.g., kidney), or additional annotations (e.g.,
650 liver) known to be important in PE. We term this augmented reference TSP+. For genes and cell
651 types measured in Tabula Sapiens v1.0 (TSP), we defined a given gene Y as specific to cell-type
652 X if Gini(Y) ≥ 0.8 and max mean expression for Y is in cell-type X. We combined annotations for
653 all neutrophil and endothelial subtypes as these were based on manifold clustering and it was
654 unclear if the subtypes were truly distinct enough to be distinguished at a whole-body level for our
655 purposes. For genes and cell types described in individual tissue single-cell atlases, we required
656 that a gene be differentially expressed in the specific single cell atlases and tissue specific per the
657 HPA (Gini ≥ 0.6). The following single cell atlases were used for each organ: 1) Placenta [64,65] 2)
658 Liver [66] 3) Kidney [67] 4) Heart [68] 5) Brain [69].
659
660 For TSP+, we then took the union of TSP and individual atlas gene annotations. A small number
661 of genes had conflicting double annotations in TSP as compared to at most one individual tissue
662 single cell atlas. In these rare instances, which most often occurred for genes related to cell-types
663 missing in TSP (e.g., placental or brain cell-types), we preferred the individual single-cell atlas
664 label to TSP.
665

666 ***Determining cell type and tissue of origin***
667 We determined whether a given cell-type or tissue was enriched in PE by comparing PE DEGs
668 with cell-type and tissue gene profiles using a hypergeometric test. For every tissue (HPA) or cell-
669 type (TSP+) with at least 2 DEGs specific to it, we performed the following. First, we defined a
670 hypergeometric distribution (scipy.stats.hypergeom, (v 1.5.1)) with the following parameters
671 where category refers to tissue when using HPA and cell-type when using TSP+: M = Number of
672 genes specific to any category, n = Number of genes specific to this category, N = number of DEGs
673 in this k-means longitudinal cluster specific to this category. Next, we estimated a p-value using
674 the survival function (1-CDF) for the specified distribution. Specifically, a p-value is defined as
675 the cumulative probability, prob(X>(n_DEGs_specific_to_this_category–1)), that the distribution
676 takes a value greater than the number of DEGS specific to this category – 1. Finally, once we
677 estimated a p-value for every cell-type (TSP+) or tissue (HPA) identified in each DEG k-means
678 longitudinal cluster, we adjusted for multiple hypotheses using Benjamini-Hochberg and a
679 significance threshold of 0.05.
680
681 ***Defining relative signature score per cell type or tissue***
682 We define a signature score as the sum of logCPM values over all genes in a given tissue or cell-
683 type gene profile. We required that a cell type or tissue gene profile have at least 5 specified genes
684 to be considered for signature scoring in cfRNA. Genes were defined as specific to a given tissue
685 based on the reference, HPA strict, and to a given cell type, based on the reference TSP+ (see
686 "Defining cell-type and tissue-specific genes" for details).
687
688 To account for our prior observation that baseline cfRNA levels vary per subject – the consequence
689 of biological and technical (e.g., sample processing) factors, we chose to calculate relative as
690 opposed to absolute signature scores. For each subject for which the post-partum sample passed
691 sample QC (see "Sample quality filtering" for details), we estimated a relative signature score
692 defined as the difference between the signature score at a given gestational time point and the post-
693 partum sample. For both Discovery and Validation 1, 49 NT and 24 PE subjects had a post-partum
694 sample that survived sample QC. After normalization, all samples at post-partum had a similar
695 baseline (0). We note that one can define a relative signature score based on any sampled time
696 point for a given person. We chose the post-partum sample because we were interested in tracking
697 maternal organ health over gestation.
698
699 Finally, we scaled (i.e., z-score) the relative signature scores for a given cell type or tissue by
700 dividing by the interquartile range, a robust alternative to standard deviation, using the
701 sklearn.preprocessing class, RobustScaler. This accounted for differing gene profile lengths and
702 gene expression levels, and allowed us to compare both different cell-type and tissue contributions
703 and case groups per cell-type or tissue.
704
705 Having defined a relative signature score per cell-type and tissue, we visualized average behavior
706 (median) and the 75% CI, a non-parametric estimation of standard deviation, (bootstrapped
707 relative signature score per case group and timepoint using 1000 iterations) using Seaborn line plot
708 (v 0.10.0).
709 Functional enrichment ***analysis***
710 Functional enrichment analysis was performed using the tool, GProfiler (v1.0.0) for the following
711 data sources, Gene ontology: biological processes and cellular compartments (GO:BP, GO:CC,

712 released 2021-05-01), Reactome (REAC, released 2021-05-07), and Kyoto Encyclopedia of Genes
713 and Genomes (KEGG, released 2021-05-03). To identify GO terms, we excluded electronic GO
714 annotations (IEA) and used a custom background of only the 7160 genes that were included in DE.
715 We then performed the recommended multiple hypothesis correction (g:SCS) with an experiment
716 wide significance threshold of a = 0.05 [70].
717
718 ***Logistic regression feature selection and training***
719 To build a robust classifier that can identify mothers at risk of PE at or before 16 weeks of
720 gestation, we first pre-selected features using the set of 330 DEGs when contrasting PE vs NT (see
721 design 2 in "Differential expression analysis" and Supplementary Note 2) as a starting point.
722
723 We normalized gene measurements using a series of steps. First, to correct for batch effect, where
724 we define batch as a set of samples processed at the same time by a distinct group (e.g., Discovery
725 cohort = batch, Del Vecchio and colleagues' cohort = batch), we centered the data by subtracting
726 the median logCPM per gene for a given cohort. Next, we scaled gene values for each cohort using
727 its corresponding interquartile range in the Discovery cohort. Finally, to account for sampling
728 differences across sample, we used an approach similar to when analyzing RT-qPCR data, and
729 normalized data using multiple internal control (i.e., housekeeping) genes. On a per sample basis,
730 we subtracted the median, normalized logCPM value (centered and scaled) for all internal control
731 genes, which we define as 66 genes for which the measured value did not change across PE vs NT
732 comparisons (All genes with adjusted p-value > 0.99 for PE vs NT, Design 2). When calculating
733 the median value for all internal control genes, we excluded any 0 logCPM values as these were
734 likely the consequence of technical dropout.
735
736 Model training then used the Discovery cohort alone split into 80% for hyperparameter tuning and
737 20% for model selection and consisted of two stages – further feature pre-selection based on two
738 metrics followed by the construction of a logistic regression model with an elastic net penalty.
739 Using a split Discovery cohort for training mitigated overfitting even though all Discovery samples
740 were used for differential expression, which defined the initial feature set.
741
742 For feature pre-selection, we calculated logFC values using the 80% Discovery split for all 330
743 genes for PE vs NT. We focused on two practical metrics measured across the 80% split of
744 Discovery samples collected on or before 16 weeks of gestation: gene change size (|logFC|) and
745 gene change stability (CV). All model hyperparameters were then tuned using AUROC as the
746 outcome metric and 5-fold cross validation. Next, we selected the best model including tuned
747 feature pre-selection cutoffs again using AUROC. Specifically, we calculated an AUROC score
748 for both the 80% and 20% Discovery splits separately, and the selected model achieved the best
749 score on both splits
750
751 Finally, we tuned the probability threshold, P, at which a sample is labeled as at risk of PE if
752 prob(PE) ≥ P using the entire Discovery cohort. To do so, we constructed a receiver operator
753 characteristic curve (ROC) and calculated the false positive rate (FPR) and true positive rate (TPR)
754 at different thresholds, P_i,. We identified the threshold, P_i, at which FPR=10%, and round to the
755 nearest 5 (e.g., 0.37 would become 0.35). This yielded a tuned threshold of P = 0.35. All
756 classifications as negative or positive were then made based on this threshold.
757

To understand the importance of each gene feature, we trained a separate logistic regression model for a subset of all possible feature subset (307 combinations out of a total of 262143 for 1–17 genes). No feature pre-selection was performed for this sub-analysis. All model hyperparameters were tuned as previously described. We defined a gene subset as weakly predictive if the model yielded an AUROC > 0.5 on the test set (Validation 2).

In all cases, performance metrics were assessed as described below (see next section) and used Scikit-learn (v 0.23.2),

Performance metric analysis

Model performance was assessed using several statistics including sensitivity, specificity, PPV, NPV, and AUROC. Given a 2x2 confusion matrix where rows 1and 2 represent true negatives and positives and columns 1 and 2 represent negative and positive predictions respectively, we can define the value in row 1, column 1 as true negatives (TN), row 1, column 2 as false positives (FP), row 2, column 1 as false negatives (FN), and row 2, column 2 as true positives (TP). We can then define the following proportions: (1) Sensitivity = TP / (TP + FN) (2) Specificity = TN / (TN + FP) (3) PPV = TP / (TP + FP) (4) NPV = TN / (TN + FN). For each proportion, we calculated 90% CIs using Jeffrey's interval [71] and the function, proportion_confint, from statsmodels.stats.proportion. We also approximated AUC and its corresponding 90% CI using the Scikit-learn function, roc_auc_score, and the binormal approximation respectively.

Statistical analyses

All p-values reported herein were calculated using the non-parametric Mann-Whitney rank test unless otherwise stated. One-sided tests were performed where required based on the hypothesis tested.

Code/data availability

All computational analyses were performed using Python 3.6 or R 3.5, and will be available on Github. Raw and processed sequencing data will be deposited with the SRA and GEO, respectively.

Figure 1. Comparing sample, maternal, and pregnancy characteristics for NT and PE groups across all cohorts. Panels illustrate matched sample collection time (weeks) in (**A**), maternal characteristics (Top to bottom: BMI, age, and gravidity) in (**B**), matched gestational age at PE onset regardless of PE symptom severity in (**C**), and gestational age at delivery in (**D**) for Discovery, Validation 1, and Validation 2 cohorts. For (**A**), schematic depicts blood sampling across gestation and plasma isolation. X-axis represents gestational age during pregnancy and time post-delivery (weeks) thereafter (ns = not significant, * $p < 0.05$ ** $\leq 10^{-7}$). BMI data is not available for Validation 2.

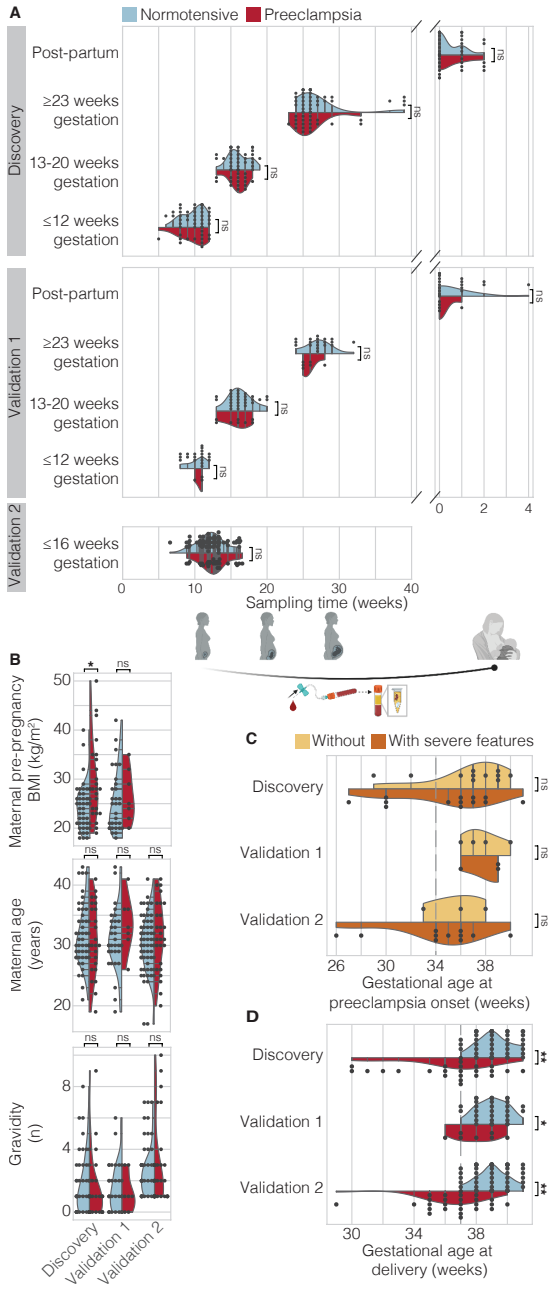

Figure 2. Before 20 weeks of gestation, changes in the cfRNA transcriptome segregate PE and NT samples and are enriched for neuromuscular, endothelial and immune cell types and tissues. (**A**) Distribution of log(Fold change) with dashed lines at log(Fold change) = ± 1 (**B**) At ≤12 and between 13–20 weeks of gestation, a subset of differentially expressed genes can separate PE and NT samples despite differences in symptom severity, PE onset subtype, and gestational age (GA) at delivery. (**C**) Comparison of log(Fold change) for DEGs between Discovery (x-axis) and Validation 2 (y-axis) reveals excellent agreement: 92%, and 94% of genes had the same logFC sign with a spearman correlation of 0.71 and 0.72 ($p < 10^{-15}$) at ≤12 and 13–20 weeks of gestation, respectively. (**D**) Across gestation, differentially expressed genes for PE as compared to NT can be described by 2 longitudinal trends: Increased in PE over gestation in orange and Decreased in PE over gestation in dark blue as revealed by k-means clustering. (**E**) Approximately 13% of DEGs are tissue- or cell-type specific when compared with the Human Protein Atlas (HPA) and an augmented Tabula Sapiens (TSP+) atlas.

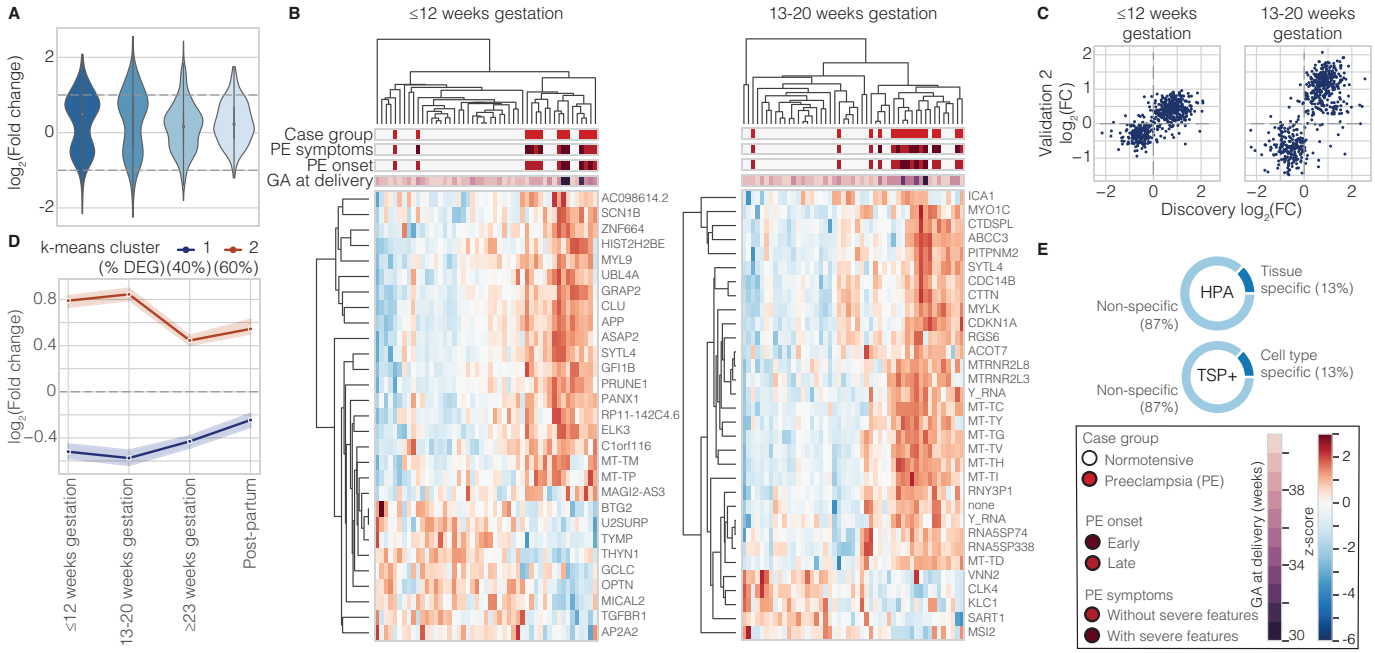

Figure 3. A subset of cfRNA changes can predict risk of PE early in gestation (**A**) Classifier performance as quantified by ROC for samples collected in early gestation between 5–16 weeks. For each cohort, including 3 validation cohorts of which Validation 2 and Del Vecchio are independent, the legend states the AUROC and the corresponding 90% CI in square brackets. (**B**) Prediction of PE incorporates cfRNA levels for 18 genes for which normalized centered $\log_2$(Fold change) trends hold across discovery, Validation 1, Validation 2, and Del Vecchio cohorts as confirmed using univariate analysis (*$p \leq 0.05$, **$p \leq 0.01$, ***$p \leq 0.005$; one-sided Mann-Whitney U-Test with Benjamini-Hochberg correction). For box-plots, center line, box limits, whiskers, and outliers represent the median, upper and lower quartiles, 1.5x interquartile range, and any outliers outside that distribution respectively. Plot limits are -8 to 4 to better visualize the main distribution.

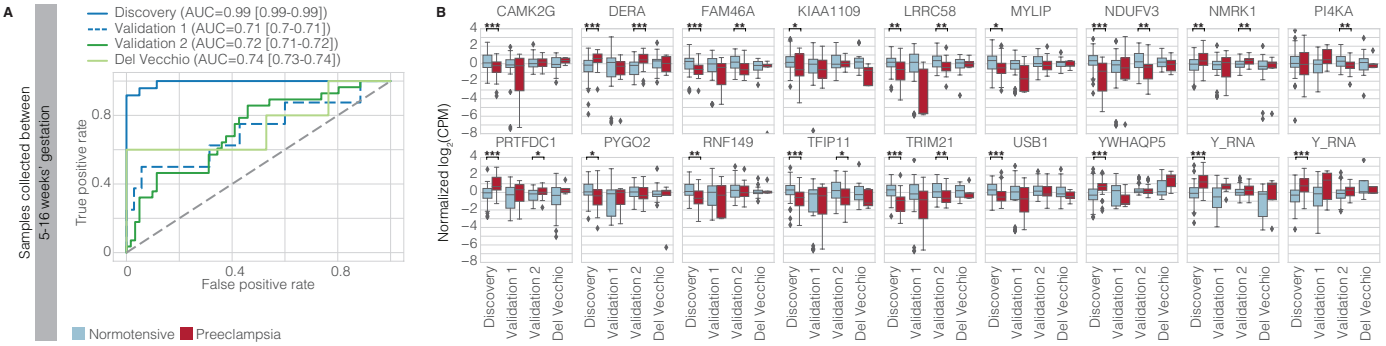

826 **Figure 4. Changes in the cfRNA transcriptome reflect PE's multifactorial nature and**
827 **pathogenesis over pregnancy prior to diagnosis.** (**A**) Across gestation, differentially expressed
828 genes for PE with as compared to without severe features (503 DEGs) can be described by 4
829 longitudinal trends as revealed by k-means clustering. Points indicate median per DEG cluster and
830 shaded region indicates 95% CI. (**B**) Comparison of organ and cell-type changes over gestation
831 for eight organ systems reflect the multifactorial nature of PE and provide a possible means to
832 monitor maternal organ health (Top to bottom: Brain, immune, placenta and kidney, heart and
833 endothelial-linked, liver and muscle). Points indicate median per sample group (NT in black, PE
834 without severe features in yellow, PE with severe features in red) and shaded region indicates 75%
835 CI.

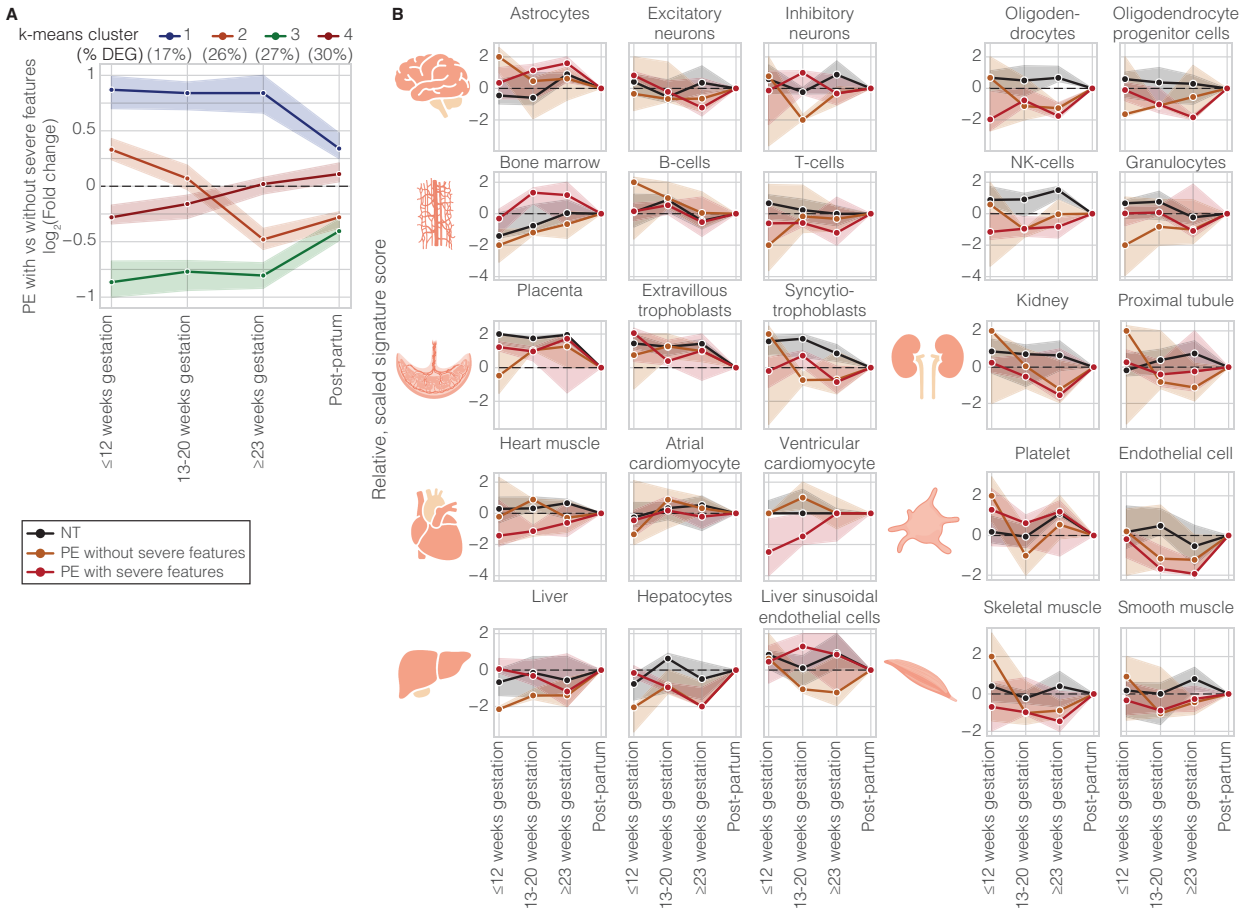

836
837

838 **Table 1. PE prediction performance metrics for samples collected early in gestation (between**
839 **5–16 weeks).** Control and case sample numbers are reported as the total sample number and in
840 parentheses, the number of samples misclassified. All other statistics including sensitivity
841 specificity, PPV, NPV, and AUROC are reported as the estimated percentage followed by the 90%
842 CI in square brackets. In Del Vecchio[1], the control group is defined as samples from any pregnant
843 mother who did not develop PE including those with other underlying or pregnancy-related
844 complications like chronic hypertension and gestational diabetes respectively. In Del Vecchio[2],
845 the control group is defined as samples strictly from NT pregnant mothers who did not experience
846 complications.
847

	Control (n)	**Case (n)**	**Sensitivity (%)**	**Specificity (%)**	**PPV (%)**	**NPV (%)**	**AUC**
Discovery	61 (9)	24 (0)	100 [92-100]	85 [77-91]	73 [59-84]	100 [96-100]	0.99 [0.99-0.99]
Validation 1	35 (11)	8 (3)	75 [46-92]	56 [43-70]	28 [15-46]	91 [77-97]	0.71 [0.7-0.71]
Validation 2	61 (19)	28 (12)	56 [42-71]	69 [59-78]	46 [32-59]	78 [68-86]	0.72 [0.71-0.72]
Del Vecchio[1] (2020)	17 (0)	5 (2)	60 [26-87]	100 [89-100]	100 [56-100]	89 [74-97]	0.74 [0.73-0.74]
Del Vecchio[2] (2020)	8 (0)	5 (2)	60 [26-87]	100 [79-100]	100 [56-100]	80 [55-94]	0.80 [0.79-0.80]

848

849 **Supplementary text**
850
851 *Supplementary note 1: Establishing quality metrics to identify sample outliers*
852 Because cfRNA measurements can be noisy [31,72], we have previously developed and reported on
853 three quality metrics that can flag sequenced cfRNA samples with poor quality [62,63]. Specifically,
854 these metrics aim to quantify unusually high levels of RNA degradation and/or DNA
855 contamination by comparing a given sample's value for any of these metrics with what we expect
856 empirically. We defined reasonable expected values for each metric based on the 95th percentile
857 for ~700 previously sequenced samples across 3 cohorts.
858
859 We found that samples with outlier values for at least one of these metrics both clustered separately
860 and served as leverage points in PCA (Fig S1A-C). To avoid introducing unwanted bias, we
861 removed these low-quality samples from any further analysis. After removing outlier samples, we
862 reran PCA and noticed that some samples continued to serve as leverage points. We suspected that
863 this may be due to genes that were poorly detected and consequently performed further filtering to
864 identify well-detected genes across the entire cohort. Specifically, we used a basic cutoff that
865 required a given gene be detected at a level of at least 0.5 CPM reads in at least 75% of samples
866 after removing outlier samples. Following this step, we retain 7,160 genes for analysis. Upon
867 inspection, we find that visualization using PCA is no longer driven by leverage points.
868
869 *Supplementary note 2: Selecting an initial feature set for machine learning*
870 We first explored whether a common gene set could describe PE with or without severe features.
871 We observed that we could separate PE from NT samples (Fig 2) irrespective of symptom severity
872 and that PE with or without severe features as compared to NT had on average the same log FC
873 (Fig S2E). With this in mind, we reran differential expression to identify a core set of genes that
874 can distinguish PE (as a binary case group) from NT (See Design 2 in methods section "Differential
875 expression analysis" for more details). This identified 330 genes that we used as an initial feature
876 set for machine learning.

Fig S1. Samples with outlier values for at least one of QC metric cluster separately from most non-outlier samples. For Discovery (**A**), Validation 1 (**B**), and Validation 2 (**C**), hierarchical clustering (left) and PCA reveals that most outlier samples cluster with negative control (NC) samples (H2O) and separately from non-outlier samples. (**D, E**) Visualization of other QC metrics like the amount of cfRNA extracted (**D**) and the percent of reads that align uniquely to the human genome (**E**). For PCA in (**A-C**), sample outliers and poorly detected genes drive PCA and serve as leverage points. The top two principal components are visualized when performed using all samples and all genes (leftmost PCA) or only samples that pass QC metrics (middle PCA) reveals that certain samples can act as leverage points. Once sample outliers and lowly detected genes are removed from the cfRNA gene matrix (rightmost PCA), the top two principal components reflect natural variance in the data and are no longer driven by a few leverage points.

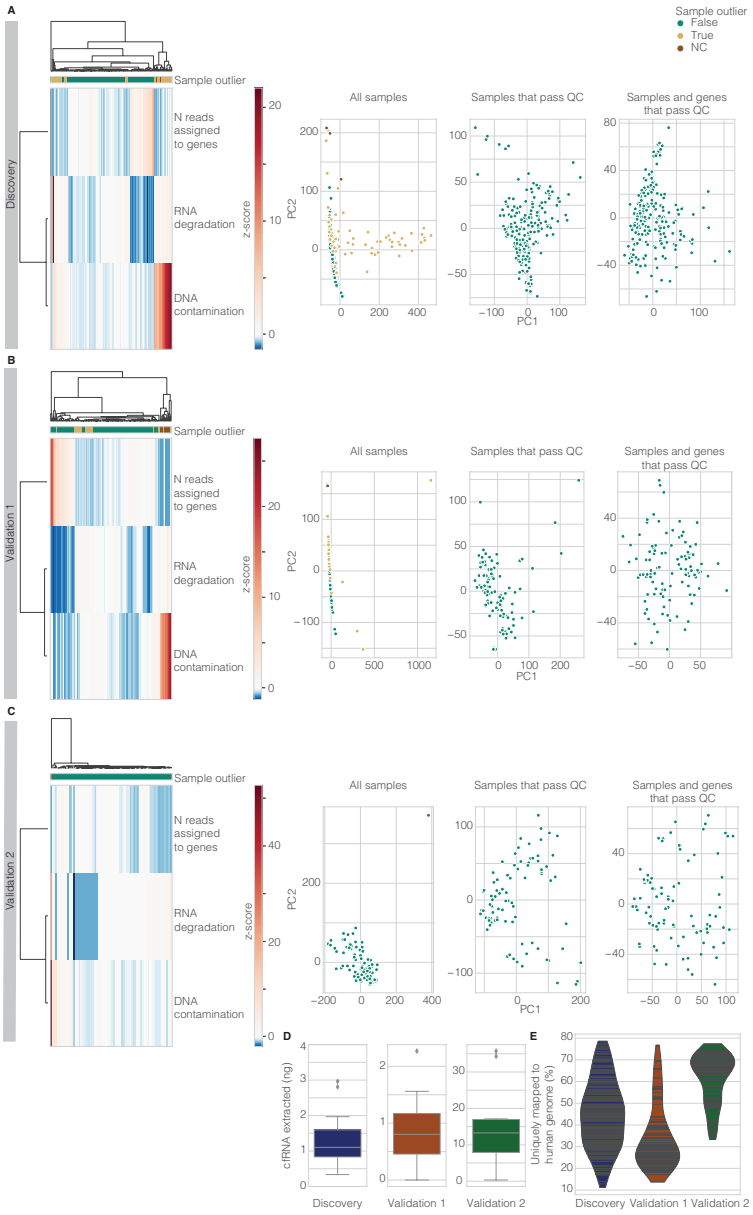

Fig S2. Across gestation prior to diagnosis, changes in the cfRNA transcriptome segregate PE and NT samples and reflect known PE biology. (**A**) Distribution of CVs with dashed line at CV = 1 for all DEGs between PE as compared to NT samples across gestation. (**B**) At ≥23 weeks of gestation and post-partum, in each sample collection period, a subset of DEGs can separate PE and NT samples despite differences in symptom severity, PE onset subtype, and gestational age (GA) at delivery. (**C**) Comparison of log(Fold change) for DEGs for PE as compared to NT between Discovery (x-axis) and Validation 1 (y-axis) reveals good agreement across gestation but not post-partum: 82%, 83%, and 60% of genes had the same logFC sign with a Spearman correlation of 0.67, 0.69, and 0.35 ($p < 10^{-15}$) at 13–20, ≥23 weeks, and post-partum, respectively. (**D**) The genes in each longitudinal trend group reflect known PE etiology as highlighted across four databases (GO biological processes, KEGG, the reactome, and GO cellular compartment). Some PE associated terms are emphasized in bold, colored text that corresponds to group color from Fig 2D (Dark blue and orange indicate decreased and increased in PE vs NT, respectively). (**E**) Comparison of log(Fold change) for DEGs for PE without severe features vs NT (x-axis) and PE with severe features vs NT in the Discovery cohort (y-axis) reveals good agreement along the y=x axis with a slope of 0.93, 1.03, 0.77, and 0.86 at ≤12 weeks, 13–20, ≥23 weeks, and post-partum, respectively.

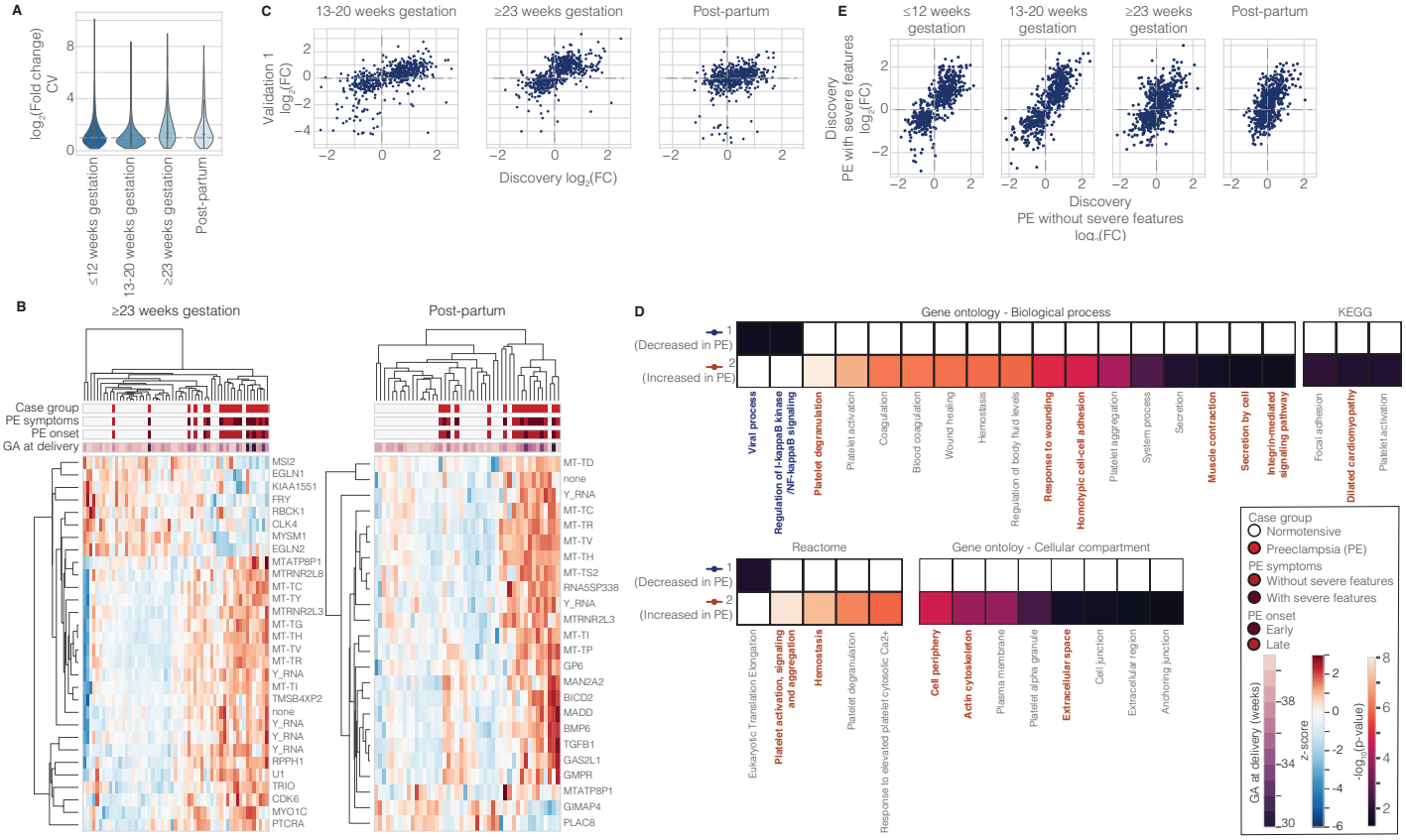

Fig S3. Across gestation and prior to diagnosis, changes in the cfRNA transcriptome identified at one timepoint can moderately segregate PE and NT samples at other timepoints. DEGs with |logFC| ≥ 1 and CV < 0.5 or 0.4 for 13–20 weeks timepoint were identified at each timepoint across gestation. Each row visualizes how well a specific DEG subset from a given sample collection period can separate PE and NT samples in all other collection periods (columns). The number of genes identified per sample collection period is highlighted along the main diagonal.

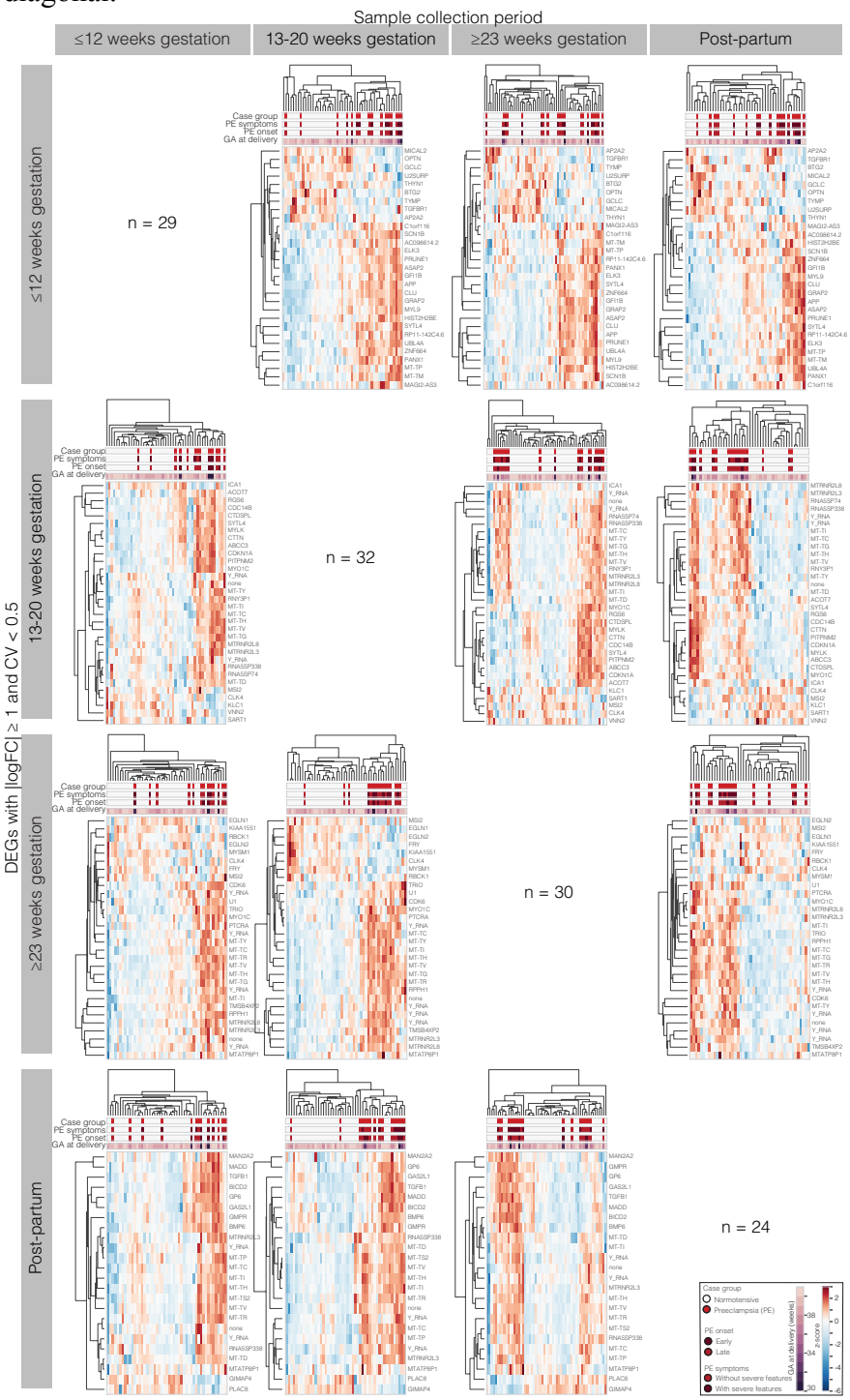

Fig S4. K-means clustering reveals meaningful longitudinal patterns. The chosen k clusters (dashed line) comparing a performance metric, the sum of squared distances, and values of k for clustering of DEGs for PE vs NT related to Fig 2D in (**A**) and DEGsfor PE with vs without severe features related to Fig 4A in (**C**). Following permutation of the data matrix prior to k-means clustering, longitudinal changes over gestation are replaced by (**B**) 2 flat lines for clustering of logFC for PE vs NT and (**D**) 4 uninformative lines for clustering of logFC for PE with vs without severe features.

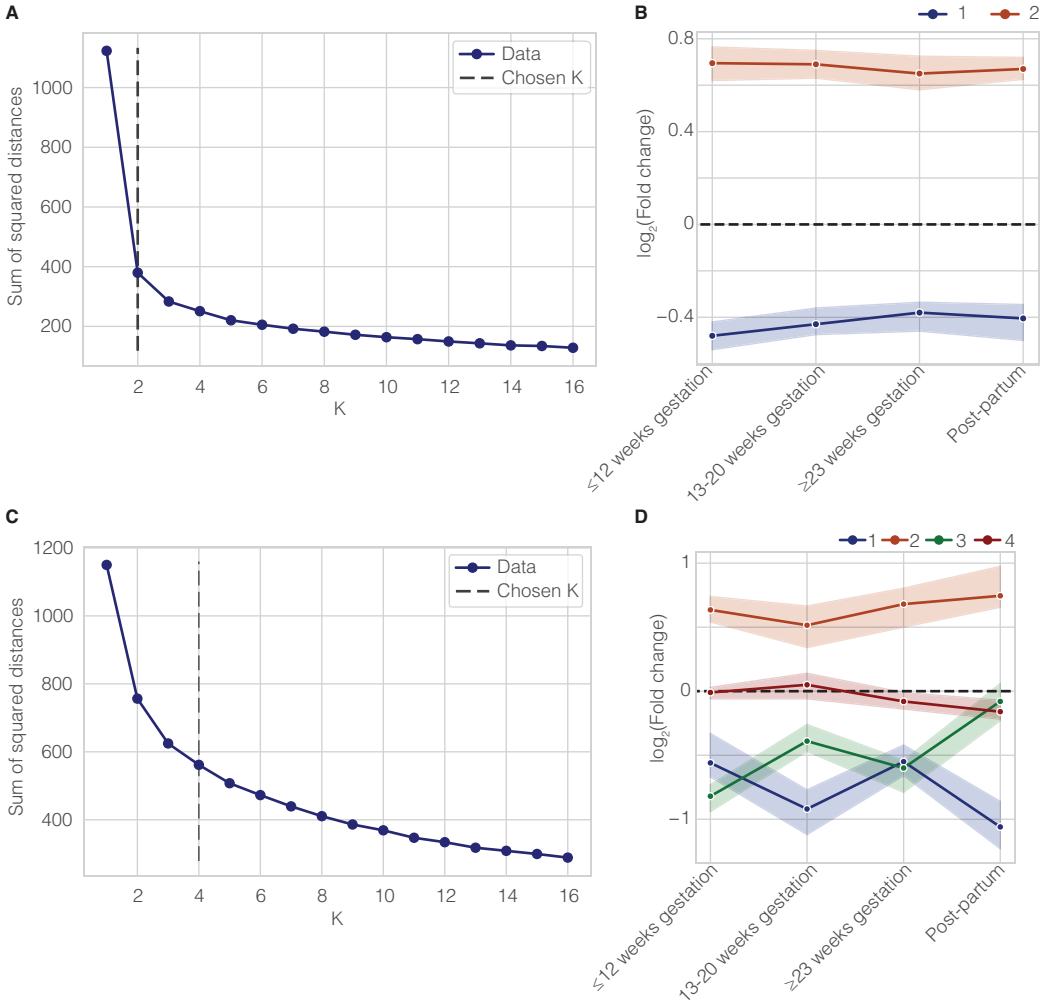

Fig S5. Examining the logisitic regression model used to predict risk of PE early in gestation (**A**) Comparison of gestational age at sample collection (weeks) for incorrectly predicted (yellow) or correctly predicted (green) samples across NT and PE groups in Discovery, Validation 1, Validation 2, and Del Vecchio shows that incorrectly predicted PE samples (false negatives) are collected at later gestational ages. (**B**) Estimated probability of PE as outputted by logistic regression for both PE and NT samples shows that the model is well-calibrated across most predictions. Dashed line at 0.35 indicates classifier cutoff where probability(PE) $\geq$ 0.35 constitutes a sample predicted as PE. (**C**) Logistic regression models trained on subsets of 1–18 genes of the initial 18 genes can moderately predict future PE onset in Validation 2 cohort with improving performance as subset size increases and as characterized by PPV, NPV, sensitivity**,** specificity, and AUROC (left to right).

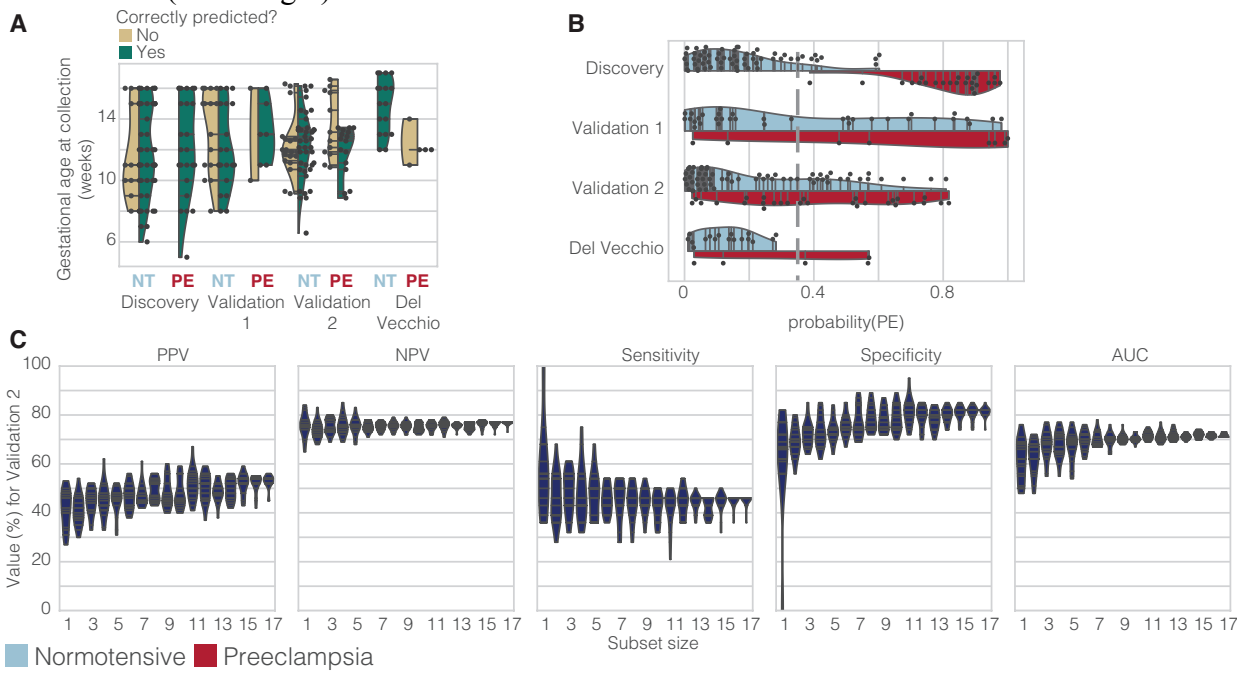

Table S1. Participant, pregnancy, and PE characteristics across both Discovery and Validation cohorts. Maternal age and BMI, gestational age (GA) at delivery, fetal weight, and GA at PE onset are reported mean ± SD. All other values are reported as percentages with the corresponding count in parentheses. Small for GA (SGA) was defined as an infant with a birthweight below the 10th centile for their GA at delivery. Pre-pregnancy BMI was not available for individuals in Validation 2 cohort. AI/AN indicates American Indians and Alaska Natives.
*adjusted $p \leq 0.05$, chi-squared (categorical) or ANOVA (continuous) test comparing all cohorts
‡ adjusted $p \leq 0.05$, chi-squared (categorical) or ANOVA (continuous) test comparing PE and NT within each cohort
† denotes that missing values were omitted from reported values for a given feature.

Maternal pre-pregnancy characteristics

		Age, years	BMI, kg/m^2	Nulliparous, % (n) *	Smoker, % (n)	History of preterm birth, % (n) *	History of PE, % (n)
Discovery	NT	32 ± 5	23 ± 3 †,‡	31 (15)	2 (1)	16 (8)	2 (1)
	PE	31 ± 6	30 ± 8 ‡	38 (9)	0 (0)	25 (6)	17 (4)
Validation 1	NT	31 ± 5	25 ± 6 †	28 (9)	3 (1)	12 (4)	9 (3)
	PE	34 ± 5	26 ± 4	29 (2)	0 (0)	29 (2)	29 (2)
Validation 2	NT	30 ± 5	NA	0 (0)	5 (3)	0 (0) ‡	0 (0)
	PE	32 ± 6	NA	0 (0)	0 (0)	50 (13) ‡	12 (3)

Maternal ethnicity/race

		Ethnicity *	Race, % (n) *					
		Hispanic	White	AI/AN	Black	Asian	Other	Unknown
Discovery	NT	22 (11)	73 (36)	0 (0)	4 (2)	20 (10)	2 (1)	0 (0)
	PE	42 (10)	50 (12)	0 (0)	4 (1)	25 (6)	0 (0)	21 (5)
Validation 1	NT	34 (11)	72 (23)	0 (0)	6 (2)	16 (5)	6 (2)	0 (0)
	PE	57 (4)	71 (5)	0 (0)	0 (0)	14 (1)	0 (0)	14 (1)
Validation 2	NT	8 (5)	59 (36)	23 (14)	5 (3)	8 (5)	0 (0)	5 (3)
	PE	4 (1)	62 (16)	23 (6)	4 (1)	4 (1)	0 (0)	4 (1)

Pregnancy characteristics

		GA at delivery, weeks *	Mode of delivery % vaginal (n) *	Multi-gestation, % (n)	Preterm delivery, % (n) *	Fetal sex, % male (n)	Fetal weight, kg *	SGA, % (n)
Discovery	NT	39 ± 1 ‡	76 (37)	0 (0)	0 ‡	53 (26)	3.4 ± 0.4 ‡	0 (0)
	PE	36 ± 3 ‡	46 (11)	12 (3)	38 (9) ‡	54 (13)	2.8 ± 0.7 ‡	4 (1)
Validation 1	NT	39 ± 1	56 (18)	3 (1)	0 (0)	53 (17)	3.4 ± 0.5 †	0 (0)
	PE	38 ± 1	57 (4)	0 (0)	14 (1)	71 (5)	3.4 ± 0.3	0 (0)
Validation 2	NT	39 ± 1 ‡	75 (46) ‡	0 (0)	0 (0) ‡	46 (28)	3.4 ± 0.4 ‡	0 (0)
	PE	37 ± 2 ‡	35 (9) ‡	8 (2)	42 (11) ‡	54 (14)	2.9 ± 0.7 ‡	8 (2)

PE characteristics

		GA at onset, weeks	Onset type, % early (n)	Symptom severity, % severe (n)
Discovery	PE	36 ± 4	25 (6)	54 (13)
Validation 1	PE	38 ± 2	0 (0)	43 (3)
Validation 2	PE	38 ± 2 †	12 (3) †	50 (13) †

951 **Table S2. Number of subjects with a given number of samples that passed QC for**
952 **Discovery and Validation 1 cohorts**

	Number of samples				
	1	**2**	**3**	**4**	**5**
Discovery	5	19	31	17	1
Validation 1	7	8	14	9	1

953
954 **Table S3. Tissue, cell-types, and genes previously implicated in PE enriched in 544 DEGs**
955 **identified when comparing PE with or without severe features and NT pregnancies.** For
956 every significantly enriched tissue or cell-type (adjusted $p \leq 0.05$, Hypergeometric test with
957 Benjamini-Hochberg correction), assigned k-means cluster (i.e., Fig 2D), reference, adjusted p-
958 values, are reported from left to right. Finally, the rightmost column lists the gene names for all
959 DEGs that were labeled as specific to a given cell-type or tissue. The last row lists gene set
960 enrichment with dbPEC, a PE specific database of genes.

K-means cluster	Specific to	Reference	Adjusted p-value	DEGs specific to cell-type or tissue
1, Decreased in PE	granulocytes	HPA	0.00026	ICAM3, PTPN6,SNX20, VNN2, LIMD2
	lymph node	HPA	0.013	CYTIP, CD48
	T-cells	HPA	0.02	TBC1D10C, TRAF3IP3
2, Increased in PE	platelet	TSP+	2.5×10^{-33}	GP9, SEPT5, AQP10, TREML1, CMTM5, GRAP2, RP11-142C4.6,BMP6, TUBB1, PTGS1, GP1BA,C6orf25, ITGA2B, PTCRA, ITGB3, RP3-370M22.8, BEND2, SEC14L5 ,ALOX12, F13A1,GP6, SLA2
	smooth muscle	HPA	0.00026	MYL9, PTGS1, MYLK, SYNM, FLNA
	total PBMC	HPA	0.00077	GP9, TREML1, TUBB1
	oligodendrocytes	TSP+	0.005	PCSK6, SH3TC2
	granulocytes	HPA	0.02	BIN2, GFI1B, ITGA2B, MTRNR2L12, NFE2
	excitatory neurons	TSP+	0.02	MTURN, NRGN
	mesenchymal stem cell	TSP+	0.03	COL6A3, NID1
	capillary aerocyte	TSP+	0.03	CLDN5, ESAM
	PE	dbPEC	0.006	CLU, ICAM3, TGFB1, IGF2, ADIPOR2, CDKN1A, GPX1, TGFBR1, RXRA, IFNGR2, JUN, PTGS1, F2R, NFKB1, GAPDH, SELP, NFKB2, ILK, GP9, ITGB3, CLDN5, ITGB1, ATP2A3, PDGFA, EGLN1, EGLN2, GP1BA, ACTB, VDR, CASP8

961

962 **Table S4. PE prediction relies on the cfRNA levels of 18 genes.** For every gene, symbol,
963 ENSEMBL ID, full name, odds ratio (OR) based on the logistic regression coefficient, and if
964 available, a subset of GO biological processes and molecular functions (if available) are reported
965 from left to right.

Gene	ENSEMBL	Name	Odds ratio	Biological process [GO]	Molecular function [GO]
CAMK2G	ENSG00000148660	calcium/calmodulin dependent protein kinase II gamma	0.65	nervous system development, protein phosphorylation, regulation of neuron projection development, regulation of skeletal muscle adaptation, insulin secretion, cell differentiation	calcium-dependent protein serine/threonine phosphatase activity, identical protein binding, protein homodimerization activity,
DERA	ENSG00000023697	deoxyribose-phosphate aldolase	1.07	pentose-phosphate shunt, deoxyribose phosphate catabolic process	deoxyribose-phosphate aldolase activity, protein binding
FAM46A	ENSG00000112773	terminal nucleotidyl transferase 5A	0.91	mRNA stabilization, response to bacterium	RNA adenylyltransferase activity, protein binding, RNA binding
KIAA1109	ENSG00000138688	KIAA1109	0.89	synaptic vesicle endocytosis, regulation of epithelial cell differentiation, endosomal transport,	protein binding
LRRC58	ENSG00000163428	leucine rich repeat containing 58	0.79		
MYLIP	ENSG00000007944	myosin regulatory light chain interacting protein	0.94	nervous system development, regulation of low-density lipoprotein particle receptor catabolic process, ubiquitin-dependent protein catabolic process, negative regulation of neuron projection development	ubiquitin protein ligase activity, cytoskeletal protein binding, protein binding, metal ion binding, ubiquitin-protein transferase activity
NDUFV3	ENSG00000160194	NADH:ubiquinone oxidoreductase subunit V3	0.66	mitochondrial electron transport, NADH to ubiquinone	NADH dehydrogenase (ubiquinone) activity, protein binding, RNA binding
NMRK1	ENSG00000106733	nicotinamide riboside kinase 1	1.42	NAD metabolic process, phosphorylation, NAD biosynthetic process	ribosylnicotinamide kinase activity
PI4KA	ENSG00000241973	phosphatidylinositol 4-kinase alpha	0.9	multi-organism membrane organization, phosphorylation, viral replication complex formation and maintenance, signal transduction	kinase activity, phosphatidylinositol kinase activity, protein binding

PRTFDC1	ENSG00000 099256	phosphoribosyl transferase domain containing 1	1.32	guanine salvage, GMP catabolic process, purine ribonucleoside salvage	protein homodimerization activity, hypoxanthine phosphoribosyltransferase activity
PYGO2	ENSG00000 163348	pygopus family PHD finger 2	0.95	positive regulation of chromatin binding, developmental growth, lens development in camera-type eye, regulation of histone H3-K4 methylation, mammary gland development	chromatin binding, protein binding, metal ion binding, histone acetyltransferase regulator activity, histone binding
RNF149	ENSG00000 163162	ring finger protein 149	0.82	ubiquitin-dependent protein catabolic process, regulation of protein stability, protein ubiquitination,	ubiquitin protein ligase activity, metal ion binding
TFIP11	ENSG00000 100109	tuftelin interacting protein 11	0.9	biomineral tissue development, negative regulation of protein binding, spliceosomal complex disassembly, mRNA splicing, via spliceosome,	protein binding, nucleic acid binding
TRIM21	ENSG00000 132109	tripartite motif containing 21	0.88	negative regulation of protein deubiquitination, regulation of protein localization, regulation of gene expression, protein monoubiquitination,	zinc ion binding, transcription coactivator activity, identical protein binding
USB1	ENSG00000 103005	U6 snRNA biogenesis phosphodiesterase 1	0.85	U6 snRNA 3'-end processing, RNA splicing,	poly(U)-specific exoribonuclease activity
Y_RNA	ENSG00000 201412	Y RNA	1.85		
Y_RNA	ENSG00000 238912	Y RNA	1.08		
YWHAQP5	ENSG00000 236564	YWHAQ pseudogene 5	1.09		

968 **Table S5. Logistic regression models trained on some subsets of 1–18 genes of the initial 18**
969 **genes can predict future PE onset with nearly equivalent performance metrics.** The associated
970 performance metrics for each data split and some high-performing gene subsets is reported
971 including sensitivity (Sens), specificity (Spec), PPV, NPV, and AUROC, which are reported as
972 the estimated percentage. Only a few, illustrative examples are shown here.
973

Subset	*Size*	**Validation 2**				
		PPV	*NPV*	*Sens*	*Spec*	*AUROC*
DERA	1	48	84	75	62	0.76
TRIM21, PI4KA	2	44	76	54	69	0.71
TRIM21, Y_RNA, DERA	3	50	78	54	75	0.77
TRIM21, USB1, PYGO2, DERA	4	50	73	32	85	0.71
LRRC58, KIAA1109, MYLIP, USB1, NMRK1	5	48	78	54	74	0.70
Y_RNA, NDUFV3, KIAA1109, MYLIP, USB1, RNF149, PRTFDC1, PI4KA, NMRK1, YWHAQP5, Y_RNA	11	67	72	21	95	0.75

974

975 **Table S6. Tissue and cell-types enriched in 503 DEGs identified when comparing PE with**
976 **as compared to without severe features.** For every significantly enriched tissue or cell-type
977 (adjusted $p \leq 0.05$, Hypergeometric test with Benjamini-Hochberg correction), assigned k-means
978 cluster (i.e., Fig 4A), reference, adjusted p-values, are reported from left to right. Finally, the
979 rightmost column lists the gene names for all DEGs that were labeled as specific to a given cell-
980 type or tissue.
981

K-means cluster	Specific to	Reference	Adjusted p-value	DEGs specific to cell-type or tissue
1, Increased across gestation for severe PE	naive b cell	TSP+	0.0002	TCL1A,TNFRSF13C
	B-cells	HPA	0.002	FCMR,TCL1A
	neutrophil	TSP+	0.002	PADI4,MEFV,DOK3
	bone marrow	HPA	0.01	PADI4,DOK3
	endothelial cell	TSP+	0.04	PDE2A,VWF
2, Increased and then decreased in early and late gestation respectively for severe PE	granulocytes	HPA	0.0007	SELL,HK3,MXD1,ALPL
	neutrophil	TSP+	0.02	FCN1,HK3
4, Decreased across gestation for severe PE	thymus	HPA	0.01	CARMIL2,ARHGAP15

982
983 **File S1. Table of 89 differentially expressed genes included in Fig 2B, S2B heatmaps.** For
984 every gene, the symbol, ENSEMBL ID, sample collection groups for which the gene passed cutoff
985 thresholds, full name, ENSEMBL gene type, and a subset of GO biological processes and
986 molecular functions are reported.
987
988 **File S2. Table of all significant GO terms related to 544 DEGS for PE with or without severe**
989 **features as compared with NT.**
990

991 Bibliography
992

993 1. Centers for Disease Control and Prevention (CDC). Healthier mothers and babies. *MMWR*
994 *Morb. Mortal. Wkly. Rep.* **48,** 849–858 (1999).
995 2. Basso, O. *et al.* Trends in fetal and infant survival following preeclampsia. *JAMA* **296,**
996 1357–1362 (2006).
997 3. Behrman, R. E., Butler, A. S. & Institute of Medicine (US) Committee on Understanding
998 Premature Birth and Assuring Healthy Outcomes. Societal Costs of Preterm Birth. (2007).
999 4. Blencowe, H. *et al.* Born too soon: the global epidemiology of 15 million preterm births.
1000 *Reprod Health* **10 Suppl 1,** S2 (2013).
1001 5. Stevens, W. *et al.* Short-term costs of preeclampsia to the United States health care system.
1002 *Am. J. Obstet. Gynecol.* **217,** 237–248.e16 (2017).
1003 6. Beam, A. L. *et al.* Estimates of healthcare spending for preterm and low-birthweight infants
1004 in a commercially insured population: 2008-2016. *J. Perinatol.* **40,** 1091–1099 (2020).
1005 7. Say, L. *et al.* Global causes of maternal death: a WHO systematic analysis. *Lancet Glob.*
1006 *Health* **2,** e323-33 (2014).
1007 8. Petersen, E. E. *et al.* Vital Signs: Pregnancy-Related Deaths, United States, 2011-2015, and
1008 Strategies for Prevention, 13 States, 2013-2017. *MMWR Morb. Mortal. Wkly. Rep.* **68,** 423–
1009 429 (2019).
1010 9. McCarthy, F. P., Ryan, R. M. & Chappell, L. C. Prospective biomarkers in preterm
1011 preeclampsia: A review. *Pregnancy hypertension* **14,** 72–78 (2018).
1012 10. Roberge, S. *et al.* The role of aspirin dose on the prevention of preeclampsia and fetal
1013 growth restriction: systematic review and meta-analysis. *Am. J. Obstet. Gynecol.* **216,** 110–
1014 120.e6 (2017).
1015 11. Duley, L. The global impact of pre-eclampsia and eclampsia. *Semin Perinatol* **33,** 130–137
1016 (2009).
1017 12. Hutcheon, J. A., Lisonkova, S. & Joseph, K. S. Epidemiology of pre-eclampsia and the other
1018 hypertensive disorders of pregnancy. *Best Pract Res Clin Obstet Gynaecol* **25,** 391–403
1019 (2011).
1020 13. Abalos, E., Cuesta, C., Grosso, A. L., Chou, D. & Say, L. Global and regional estimates of
1021 preeclampsia and eclampsia: a systematic review. *Eur. J. Obstet. Gynecol. Reprod. Biol.*
1022 **170,** 1–7 (2013).
1023 14. Zhang, J., Meikle, S. & Trumble, A. Severe maternal morbidity associated with
1024 hypertensive disorders in pregnancy in the United States. *Hypertens Pregnancy* **22,** 203–212
1025 (2003).
1026 15. Steegers, E. A. P., von Dadelszen, P., Duvekot, J. J. & Pijnenborg, R. Pre-eclampsia. *Lancet*
1027 **376,** 631–644 (2010).
1028 16. Li, X. *et al.* Hypertensive disorders of pregnancy and risks of adverse pregnancy outcomes:
1029 a retrospective cohort study of 2368 patients. *J Hum Hypertens* (2020). doi:10.1038/s41371-
1030 020-0312-x
1031 17. Hansen, A. R., Barnés, C. M., Folkman, J. & McElrath, T. F. Maternal preeclampsia
1032 predicts the development of bronchopulmonary dysplasia. *J. Pediatr.* **156,** 532–536 (2010).
1033 18. Wang, A. *et al.* Circulating anti-angiogenic factors during hypertensive pregnancy and
1034 increased risk of respiratory distress syndrome in preterm neonates. *J. Matern. Fetal*
1035 *Neonatal Med.* **25,** 1447–1452 (2012).
1036 19. Bellamy, L., Casas, J.-P., Hingorani, A. D. & Williams, D. J. Pre-eclampsia and risk of

1037 cardiovascular disease and cancer in later life: systematic review and meta-analysis. *BMJ*
1038 **335,** 974 (2007).
1039 20. Ahmed, R., Dunford, J., Mehran, R., Robson, S. & Kunadian, V. Pre-eclampsia and future
1040 cardiovascular risk among women: a review. *J. Am. Coll. Cardiol.* **63,** 1815–1822 (2014).
1041 21. Vikse, B. E., Irgens, L. M., Leivestad, T., Skjaerven, R. & Iversen, B. M. Preeclampsia and
1042 the risk of end-stage renal disease. *N. Engl. J. Med.* **359,** 800–809 (2008).
1043 22. McDonald, S. D., Han, Z., Walsh, M. W., Gerstein, H. C. & Devereaux, P. J. Kidney disease
1044 after preeclampsia: a systematic review and meta-analysis. *Am. J. Kidney Dis.* **55,** 1026–
1045 1039 (2010).
1046 23. Hypertension in pregnancy. Report of the American College of Obstetricians and
1047 Gynecologists' Task Force on Hypertension in Pregnancy. *Obstet. Gynecol.* **122,** 1122–1131
1048 (2013).
1049 24. Goel, A. *et al.* Epidemiology and mechanisms of de novo and persistent hypertension in the
1050 postpartum period. *Circulation* **132,** 1726–1733 (2015).
1051 25. Zeisler, H. *et al.* Predictive Value of the sFlt-1:PlGF Ratio in Women with Suspected
1052 Preeclampsia. *N. Engl. J. Med.* **374,** 13–22 (2016).
1053 26. Sovio, U. *et al.* Prediction of Preeclampsia Using the Soluble fms-Like Tyrosine Kinase 1 to
1054 Placental Growth Factor Ratio: A Prospective Cohort Study of Unselected Nulliparous
1055 Women. *Hypertension* **69,** 731–738 (2017).
1056 27. Gestational hypertension and preeclampsia: ACOG practice bulletin, number 222. *Obstet.*
1057 *Gynecol.* **135,** e237–e260 (2020).
1058 28. Roberge, S. *et al.* Early administration of low-dose aspirin for the prevention of preterm and
1059 term preeclampsia: a systematic review and meta-analysis. *Fetal Diagn Ther* **31,** 141–146
1060 (2012).
1061 29. Henderson, J. T., Vesco, K. K., Senger, C. A., Thomas, R. G. & Redmond, N. Aspirin use to
1062 prevent preeclampsia and related morbidity and mortality: updated evidence report and
1063 systematic review for the US preventive services task force. *JAMA* **326,** 1192–1206 (2021).
1064 30. Whitehead, C. L., Walker, S. P. & Tong, S. Measuring circulating placental RNAs to non-
1065 invasively assess the placental transcriptome and to predict pregnancy complications.
1066 *Prenat. Diagn.* **36,** 997–1008 (2016).
1067 31. Munchel, S. *et al.* Circulating transcripts in maternal blood reflect a molecular signature of
1068 early-onset preeclampsia. *Sci. Transl. Med.* **12,** (2020).
1069 32. Tsang, J. C. H. *et al.* Integrative single-cell and cell-free plasma RNA transcriptomics
1070 elucidates placental cellular dynamics. *Proc. Natl. Acad. Sci. USA* **114,** E7786–E7795
1071 (2017).
1072 33. Del Vecchio, G. *et al.* Cell-free DNA Methylation and Transcriptomic Signature Prediction
1073 of Pregnancies with Adverse Outcomes. *Epigenetics* **16,** 642–661 (2021).
1074 34. Phipps, E. A., Thadhani, R., Benzing, T. & Karumanchi, S. A. Pre-eclampsia: pathogenesis,
1075 novel diagnostics and therapies. *Nat. Rev. Nephrol.* **15,** 275–289 (2019).
1076 35. Pennington, K. A., Schlitt, J. M., Jackson, D. L., Schulz, L. C. & Schust, D. J. Preeclampsia:
1077 multiple approaches for a multifactorial disease. *Dis. Model. Mech.* **5,** 9–18 (2012).
1078 36. Burton, G. J., Redman, C. W., Roberts, J. M. & Moffett, A. Pre-eclampsia: pathophysiology
1079 and clinical implications. *BMJ* **366,** l2381 (2019).
1080 37. von Dadelszen, P., Magee, L. A. & Roberts, J. M. Subclassification of preeclampsia.
1081 *Hypertens Pregnancy* **22,** 143–148 (2003).
1082 38. Huppertz, B. Placental origins of preeclampsia: challenging the current hypothesis.

1083 *Hypertension* **51,** 970–975 (2008).
1084 39. Raymond, D. & Peterson, E. A critical review of early-onset and late-onset preeclampsia.
1085 *Obstet Gynecol Surv* **66,** 497–506 (2011).
1086 40. Chaiworapongsa, T. *et al.* Differences and similarities in the transcriptional profile of
1087 peripheral whole blood in early and late-onset preeclampsia: insights into the molecular
1088 basis of the phenotype of preeclampsiaa. *J Perinat Med* **41,** 485–504 (2013).
1089 41. Leavey, K. *et al.* Unsupervised placental gene expression profiling identifies clinically
1090 relevant subclasses of human preeclampsia. *Hypertension* **68,** 137–147 (2016).
1091 42. Benton, S. J., Leavey, K., Grynspan, D., Cox, B. J. & Bainbridge, S. A. The clinical
1092 heterogeneity of preeclampsia is related to both placental gene expression and placental
1093 histopathology. *Am. J. Obstet. Gynecol.* **219,** 604.e1-604.e25 (2018).
1094 43. Koh, W. *et al.* Noninvasive in vivo monitoring of tissue-specific global gene expression in
1095 humans. *Proc. Natl. Acad. Sci. USA* **111,** 7361–7366 (2014).
1096 44. Vorperian, S. K., Moufarrej, M. N., Consortium, T. S. & Quake, S. R. Cell types of origin in
1097 the cell free transcriptome in human health and disease. *BioRxiv* (2021).
1098 doi:10.1101/2021.05.05.441859
1099 45. Gillich, A. *et al.* Capillary cell-type specialization in the alveolus. *Nature* **586,** 785–789
1100 (2020).
1101 46. Arck, P. C. & Hecher, K. Fetomaternal immune cross-talk and its consequences for maternal
1102 and offspring's health. *Nat. Med.* **19,** 548–556 (2013).
1103 47. Uzun, A., Triche, E. W., Schuster, J., Dewan, A. T. & Padbury, J. F. dbPEC: a
1104 comprehensive literature-based database for preeclampsia related genes and phenotypes.
1105 *Database (Oxford)* **2016,** (2016).
1106 48. Ostlund, I., Haglund, B. & Hanson, U. Gestational diabetes and preeclampsia. *Eur. J.*
1107 *Obstet. Gynecol. Reprod. Biol.* **113,** 12–16 (2004).
1108 49. Schneider, S., Freerksen, N., Röhrig, S., Hoeft, B. & Maul, H. Gestational diabetes and
1109 preeclampsia--similar risk factor profiles? *Early Hum. Dev.* **88,** 179–184 (2012).
1110 50. Nerenberg, K. A. *et al.* Risks of gestational diabetes and preeclampsia over the last decade
1111 in a cohort of Alberta women. *J Obstet Gynaecol Can* **35,** 986–994 (2013).
1112 51. Weissgerber, T. L. & Mudd, L. M. Preeclampsia and diabetes. *Curr Diab Rep* **15,** 9 (2015).
1113 52. Rey, E. & Couturier, A. The prognosis of pregnancy in women with chronic hypertension.
1114 *Am. J. Obstet. Gynecol.* **171,** 410–416 (1994).
1115 53. McCowan, L. M., Buist, R. G., North, R. A. & Gamble, G. Perinatal morbidity in chronic
1116 hypertension. *Br J Obstet Gynaecol* **103,** 123–129 (1996).
1117 54. Sibai, B. M. *et al.* The impact of prior preeclampsia on the risk of superimposed
1118 preeclampsia and other adverse pregnancy outcomes in patients with chronic hypertension.
1119 *Am. J. Obstet. Gynecol.* **204,** 345.e1-6 (2011).
1120 55. Uhlen, M. *et al.* A genome-wide transcriptomic analysis of protein-coding genes in human
1121 blood cells. *Science* **366,** (2019).
1122 56. Han, X. *et al.* Differential dynamics of the maternal immune system in healthy pregnancy
1123 and preeclampsia. *Front. Immunol.* **10,** 1305 (2019).
1124 57. Ander, S. E., Diamond, M. S. & Coyne, C. B. Immune responses at the maternal-fetal
1125 interface. *Sci. Immunol.* **4,** (2019).
1126 58. Szarka, A., Rigó, J., Lázár, L., Beko, G. & Molvarec, A. Circulating cytokines, chemokines
1127 and adhesion molecules in normal pregnancy and preeclampsia determined by multiplex
1128 suspension array. *BMC Immunol.* **11,** 59 (2010).

1129 59. Lisonkova, S. & Joseph, K. S. Incidence of preeclampsia: risk factors and outcomes
1130 associated with early- versus late-onset disease. *Am. J. Obstet. Gynecol.* **209,** 544.e1-
1131 544.e12 (2013).
1132 60. Marić, I. *et al.* Early prediction of preeclampsia via machine learning. *American Journal of*
1133 *Obstetrics & Gynecology MFM* **2,** 100100 (2020).
1134 61. Robinson, M. D. & Oshlack, A. A scaling normalization method for differential expression
1135 analysis of RNA-seq data. *Genome Biol.* **11,** R25 (2010).
1136 62. Pan, W. Development of diagnostic methods using cell-free nucleic acids. (Stanford
1137 University, 2016).
1138 63. Moufarrej, M. N., Wong, R. J., Shaw, G. M., Stevenson, D. K. & Quake, S. R. Investigating
1139 Pregnancy and Its Complications Using Circulating Cell-Free RNA in Women's Blood
1140 During Gestation. *Front. Pediatr.* **8,** 605219 (2020).
1141 64. Vento-Tormo, R. *et al.* Single-cell reconstruction of the early maternal-fetal interface in
1142 humans. *Nature* **563,** 347–353 (2018).
1143 65. Suryawanshi, H. *et al.* A single-cell survey of the human first-trimester placenta and
1144 decidua. *Sci. Adv.* **4,** eaau4788 (2018).
1145 66. Aizarani, N. *et al.* A human liver cell atlas reveals heterogeneity and epithelial progenitors.
1146 *Nature* **572,** 199–204 (2019).
1147 67. Stewart, B. J. *et al.* Spatiotemporal immune zonation of the human kidney. *Science* **365,**
1148 1461–1466 (2019).
1149 68. Litviňuková, M. *et al.* Cells of the adult human heart. *Nature* **588,** 466–472 (2020).
1150 69. Mathys, H. *et al.* Single-cell transcriptomic analysis of Alzheimer's disease. *Nature* **570,**
1151 332–337 (2019).
1152 70. Raudvere, U. *et al.* g:Profiler: a web server for functional enrichment analysis and
1153 conversions of gene lists (2019 update). *Nucleic Acids Res.* **47,** W191–W198 (2019).
1154 71. Brown, L. D., Cai, T. T. & DasGupta, A. Interval Estimation for a Binomial Proportion. *Stat*
1155 *Sci* **16,** 101–133 (2001).
1156 72. Ibarra, A. *et al.* Non-invasive characterization of human bone marrow stimulation and
1157 reconstitution by cell-free messenger RNA sequencing. *Nat. Commun.* **11,** 400 (2020).
1158